Journal of the European Ceramic Society 45 (2025) 117666

Contents lists available at ScienceDirect

Journal of the European Ceramic Society

journal homepage: www.elsevier.com/locate/jeurceramsoc

Resistance to cyclic oxidation and evolution of oxide scale in 2.5D and 3D C_f/SiC composites with Si-B-C added matrix

Ramya Krishna [a,*], A. Udayakumar [b], Rahul Mitra [a]

[a] Department of Metallurgical and Materials Engineering, Indian Institute of Technology Kharagpur, Kharagpur, West Bengal 721302, India
[b] Materials Science Division, Council of Scientific and Industrial Research - National Aerospace Laboratories, Bangalore 560017, India

ARTICLE INFO

Keywords:
C_f/SiC composites
SiC/SiBC matrix
Fibre preform architecture
Cyclic oxidation
Oxide scale

ABSTRACT

The effect of fibre preform architecture (2.5D-woven and 3D-NOOBed) on the oxidation behaviour of CVI-processed C_f/SiC composites with $(PyC/SiC)_{n=4}$ interphase and SiC/SiBC matrix has been studied using non-isothermal and cyclic exposure tests. The mass loss of 3D C_f/SiC composite by CO (g) formation exceeds that of 2.5D composite by ~33 % during heating to 1200 °C in a thermogravimetric analyser and by ~7–90 times on cyclic oxidation at 1250–1500 °C. FESEM-EDS and ToF-SIMS analyses confirm a stable borosilicate-rich oxide scale at 1400 °C, leading to > 80 % post-oxidation flexural strength retention. Sluggish SiO_2 growth kinetics and active oxidation of SiC are considered responsible for the oxide scale to be less protective at 1250 and 1500 °C, respectively. Poor strength retention (~57 %) of the 3D C_f/SiC composite exposed at 1250 °C is attributed to significant oxidation-induced damage caused by increased oxygen ingress through larger pore volume and higher interfacial area along the z-direction.

1. Introduction

The need to increase the operating temperature of the hot end load-bearing components of jet engines for increased efficiency and reduction of the NO_x/CO_x emissions has promoted the development of ceramic matrix composites (CMC) in recent years. The SiC-based CMCs reinforced with carbon fibres (C_f) or SiC fibres are the potential candidates for thermostructural applications such as nozzle flaps, nose caps, and jet vanes due to their high specific strength, low density, and oxidation resistance. Utilising these CMCs can significantly improve their fuel efficiency and thrust-to-weight ratio compared to the nickel-based super alloys [1–5]. The carbon fibres are often preferred in comparison to the SiC fibres in thermal load-bearing applications due to their superior mechanical properties, chemical compatibility with SiC at temperatures up to 2500 °C, and a relatively lower cost [1,5]. The main advantage of using the continuous fibre-reinforced CMCs for load-bearing applications is due to their non-catastrophic failure involving fibre debonding and pull-out, which is facilitated by engineering of the fibre-matrix interface to sufficiently reduce the bond strength. Fibre debonding and pull-out is accompanied by crack bridging by the fibres oriented perpendicular to the crack propagation direction, leading to sharp increases in both the crack path tortuosity as well as the total energy dissipated in fracture. The ease of fibre debonding being the root cause of graceful failure, is ensured by depositing a thin and continuous film of compliant material between the fibre and matrix called the interphase. The primary function of the compliant interphase is to deflect the cracks as well as to transfer the load from the matrix to the fibre [6]. The commonly used constituents for engineering a compliant interphase include pyrolytic carbon, a graphitic carbon deposited from a gaseous precursor, and hexagonal boron nitride. Both graphitic carbon and hexagonal boron nitride possess a stacked crystal structure, wherein a weak van der Waals bond exists between the layers deposited on the fibre surface.

Chemical vapour infiltration (CVI) is the most promising technique for developing the optimised interphases, as it ensures stoichiometric and precise deposition with control over the microstructure. Another advantage of CVI is that it utilises low temperature and pressure to produce components with complex shapes without compromising mechanical properties [7]. However, the C_f/SiC composite produced via CVI has residual pores located among the fibre bundles as well as micro-cracks in the matrix, resulting from the difference between the thermal expansion coefficients of fibre and matrix. These micro-cracks can act as the paths for easy penetration of oxygen, leading to carbon fibre oxidation with degradation of the thermomechanical properties

* Corresponding author.
E-mail address: ramyakrishna0507@gmail.com (R. Krishna).

https://doi.org/10.1016/j.jeurceramsoc.2025.117666
Received 25 February 2025; Received in revised form 5 June 2025; Accepted 10 July 2025
Available online 11 July 2025

[8]. Hence, from a long-term application point of view, the CMCs should be engineered in such a way that both their damage tolerance and oxidation resistance are adequately improved.

Modifying the matrix and interphase to protect the reinforcement fibres from oxidation is a favourable technique for achieving superior oxidation resistance. Another method is the application of a suitable protective coating [9,10]. The primary objective of the coating or the modified matrix is to act as an oxygen scavenger and contribute to the formation of a protective oxide scale, which can effectively prevent the oxygen from reaching the reinforcement carbon fibre, such that its degradation by oxidation can be inhibited.

The incorporation of boron-bearing species in the SiC matrix has been reported to enhance the oxidation resistance of C_f/SiC composites prepared through CVI. This method involves the modification of SiC-containing matrix with Si-B-C, B_4C. BN, SiB_4 and Si-B-C-N by using appropriate gaseous precursors. The matrices modified in such a way form B_2O_3 or $B_2O_3.xSiO_2$, when exposed to an oxidising atmosphere over a temperature range of 600–1400 °C [11–17]. The B-modified matrix of these ceramics is known to form a viscous, self-healing borosilicate scale with sufficient plasticity and fluidity to fill cracks and pores in the oxide scale, and retard the ingress of oxygen. The self-healing ability of the borosilicate scale has been considered responsible for significant improvement in oxidation resistance of the SiC_f/SiC composite having $(SiC/SiBC)_m$ matrix within the temperature range of 900–1200 °C, as reported by Viricelle et al. [18]. In the 3D C_f/SiC composite with SiC/BC/SiC (amorphous boron carbide) coating, the strength retained after exposure at 1200 °C for 100 h has been reported as ~82.6 % of that measured at room temperature [19].

Previous studies have reported that both single-layer and multilayered coatings consisting of SiC [20,21] and Si-B-C [22] play an important role in strength retention at oxidising atmospheres. The SiC has been widely used as a coating, because of its chemical compatibility with both SiC and Si-B-C matrix as well as the carbon fibres [10]. On the other hand, a seal coating of Si-B-C is expected to undergo rapid oxidation to form a mixture of SiO_2 and B_2O_3, in which the latter oxide would be volatilised at high temperatures, leading to the formation of a porous oxide scale. Therefore, keeping the Si-B-C layer within the matrix is expected to not only restrict the volatilisation of B_2O_3, but also localise the glass formation within the cracks formed on subjecting to external load. Such an approach is preferred to relying solely on an external coating, which may fail to prevent oxidation in applications where the cracks formed by static or dynamic loads may progress to the underneath composite [9].

In addition to matrix modification, optimisation of the interphase also leads to enhancement of the oxidation resistance. Incorporating a multilayered interphase having alternate layers of PyC and SiC, such that the PyC serves as a compliant layer and the SiC shields the PyC from oxidation, results in a composite that is both damage-tolerant and load-bearing, with enhanced oxidation resistance [23–28]. In addition to the structure and composition of interphase, matrix and surface coating, the fibre architecture plays an essential role in the properties of these composites. The relevance of fibre preform architecture is based on its influence on the uniformity of matrix impregnation, which in turn depends on the nature of porosity, precisely the size and distribution of pores. An earlier study by the authors has shown a significant difference between the nature of porosity in 2.5D (preform obtained by stitching of 2D layers along the z-direction) and 3D NOOBed (preform of non-interlacing fibres subjected to orthogonally orientated binding) C_f/SiC composites, particularly size, orientation and distribution of inter-bundle as well as inter-fibre pores [29]. It is well accepted that the interconnected porosity plays an important role in permitting the ingress of atmospheric oxygen, which in turn is responsible for environmental degradation by oxidation and the accompanying reduction of strength.

Quite a few reports on the high-temperature oxidation behaviour of C_f/SiC composites exist in the literature [11,30–33]. Naslain et al. have shown that the carbon fibres are consumed by the through-thickness oxidation of 2D C_f/SiC composites, when exposed at intermediate temperatures (600–1000 °C). However, the environmental degradation tends to be confined only to the vicinity of the composite surface at higher temperatures (>1000 °C), because of the rapid growth in self-healing and protective scale of SiO_2 formed by the oxidation of SiC matrix [34]. Therefore, considering the need to protect the C_f/SiC composites during exposure at 700–1300 °C, a hybrid coating with B_2O_3, B_4C and SiBC has been developed. However, an outer coating of B_2O_3 is not feasible due to its volatilization. A previous study has compared the oxidation protection of multilayered SiC/B/SiC coating with SiC/SiC/SiC coatings for the 3D C_f/SiC composite. After exposure at 700 °C, the composite with SiC/B/SiC coating has exhibited a strength retention of 87 %, whereas that with SiC/SiC/SiC coatings has retained only 77 % of the room temperature strength. However, the SiC/SiC/SiC coated composite has outlived the SiC/B/SiC composite significantly on exposure beyond 1300 °C [35]. Moreover, it has been reported that the oxidation kinetics of C_f/SiC composites at temperatures > 1000 °C is controlled by the diffusion rate of oxygen through the coating defects [36,37].

Despite the extensive research carried out on the oxidation behaviour of C_f/SiC composites during the past few decades, the impact of fibre architecture, particularly NOOBing, on the long-term oxidation behaviour of these composites remains unexplored. As a result, only limited information is available about the formation of oxide scale in the C_f/SiC composites with NOOBed fibre architecture [10]. In this regard, it is needless to emphasise that the formation of oxide scale is influenced by the composition of coating and matrix, as well as the size and distribution of pores. A thorough analysis of the oxide scale's compositional evolution, stability as well as structural integrity during exposure is important to assess its ability to provide protection against further oxidation. Evaluation of the oxidation rates is also critical, as it directly impacts both the lifespan of the materials and the extent to which their flexural strengths are deteriorated due to high temperature exposure.

Considering the threat of environmental degradation during exposure at high temperatures along with multiple cycles of heating and cooling, the present study has focused on the oxidation behaviour of 2.5D and 3D C_f/SiC composites subjected to 10 cycles of 10 h exposure at 1250 °C, 1400 °C or 1500 °C. Further, the damage caused by cyclic oxidation has been quantified by evaluating the post-exposure flexural strength and comparing it with that obtained in the as-received condition. The test temperatures have been chosen, keeping in mind the application of these composites in hot end components of aero-engines operating at temperatures > 1200 °C. The oxide scales and cross-sections of these composites have been examined using the Time of Flight - Secondary Ion Mass Spectrometer (ToF-SIMS) with depth profiling by Ar ion sputtering to assess the penetration of oxygen into these composites as well as understand how the structure and composition of the oxide scale varies with the fibre preform architecture. The findings of the present study provide a deep insight about the dependence of oxidation kinetics on fibre architecture, the combined effect of SiC seal coating, multilayered interphase, and SiBC matrix on the oxide scale evolution, as well as the degradation of strength jointly by oxidation and thermal shock caused by cyclic exposure.

2. Experimental methods

2.1. Materials and preparation

The 2.5D preforms were fabricated by laying of multiple pieces of (lay-up technique) the 8H satin-weave cloth containing T300 3 K carbon fibres (Toray International, Japan) one above the other, followed by stitching them in the z-direction using the same fibre. On the other hand, the 3D preforms were prepared by NOOBing using the above-mentioned carbon fibres as the raw material. The processing route used for fabricating these composites was isothermal chemical vapour infiltration

(CVI). The composites were manufactured using a CVI reactor at the CSIR-National Aerospace Laboratories (NAL) in Bengaluru, India. The fibres were initially coated with alternate layers of PyC and SiC to obtain the $(PyC/SiC)_{n=4}$ interphase by sequentially carrying out the chemical reactions required for each of these layers four times [38].

The PyC, which was infiltrated into the C_f preforms, was derived by the pyrolysis of methane (CH_4, 99.97 %, Bhuruka Gases Limited, Bangalore, India) at a temperature of 1200 °C inside a chamber having a gas pressure of 1–2 mbar. The SiC required as a part of the interphase and subsequently the matrix of the composites was deposited from methyltrichlorosilane (MTS) (CH_3SiCl_3-99.5 % Lakshmeetech and Applied Materials, Chennai, India) through its reaction with hydrogen (H_2,99.997 %, Inox Air products, Bangalore) at 960 °C inside the CVI chamber at a pressure of ~1–2 mbar. The CVI cycles for SiC matrix infiltration were started after the end of interphase deposition process, as discussed above, and continued for a duration of 530 h. The addition of boron trichloride (BCl_3, 99.7 %, Praxair) gas, together with MTS and hydrogen, was carried out for the infiltration of Si-B-C throughout the interval of 415–465 h, as an intermediate step during the in-situ formation of SiC matrix by CVI. The 2.5D panels with dimensions of 270 mm × 250 mm × 3.5 mm and 3D panels with dimensions of 290 mm × 290 mm × 5.5 mm were taken out of the CVI reactor after their densification.

The C_f/SiC composites manufactured through NOOBing are generally found to exhibit greater thickness compared to the 2.5D woven composites, owing to the difference between their structural characteristics. The 3D NOOBed composites are fabricated by orthogonally orienting three sets of yarns, which on binding, do not undergo interlacing or interlooping [39]. As a result, the NOOBed composites possess a through-thickness fibre arrangement, in which each fibre yarn is separated all along its length from its nearest neighbour of similar orientation by an orthogonally oriented yarn of the same diameter. On the contrary, the woven clothes used in fabricating the 2.5D composites have a pair of mutually orthogonal yarns which during weaving are interlaced or interlooped with respect to one another, resulting in tighter packing and flattened appearance. On stitching, the stacked woven clothes are compressed along the vertical direction and therefore exhibit less thickness compared to the 3D NOOBed composite. In other words, the packing density is more and porosity is less along the vertical (z) direction of the 2.5D fibre preform in comparison to that of 3D preform. Consequently, the 2.5D C_f/SiC composite panels achieve a thickness of approximately 3.5–4 mm, whereas the 3D C_f/SiC panels attain a thickness of 5.5–6 mm after SiC infiltration.

Following the fabrication by CVI process, different test coupons of specified dimensions were fabricated using waterjet cutting. Subsequently, these cleaned and chamfered test coupons were introduced into the CVI reactor to apply the SiC seal coating via chemical vapour deposition (CVD). Each of the process steps mentioned above has been described in detail in a few earlier publications [29,38].

2.2. Oxidation tests

2.2.1. Non-isothermal oxidation tests

Non-isothermal oxidation tests were conducted using a thermogravimetric analyzer (TG-DTA, model: Perkin Elmer, USA). For the purpose of TGA study, specimens weighing less than 14 mg were heated inside an alumina crucible in air from 28 °C to 1200 °C at 10 °C per minute. The precise change in mass with temperature was measured continuously using the TGA.

2.2.2. Cyclic oxidation tests

Cyclic oxidation of 2.5D and 3D C_f/SiC composites was carried out at 1250 °C, 1400 °C and 1500 °C in a horizontal tube furnace (Bysakh & Company, Kolkata, India). Rectangular bars of dimension 75 mm × 12 mm × 3.5 mm and 105 mm × 17 mm × 5.5 mm were used as samples for cyclic oxidation tests carried out on 2.5D and 3D C_f/SiC composites, respectively. The samples were placed in the hot zone of the furnace, and were exposed at each set temperature for a dwell time of 10 h. After each 10 h exposure, the samples were removed from the furnace, cooled in laboratory air to room temperature, and then the mass was measured using a precision analytical balance (Model Sartorius GR-202). Subsequently, the sample was loaded back into the furnace. This procedure was repeated for ten cycles, such that the net duration of exposure at each of the test temperatures was 100 h. In order to minimise the effect of size difference between the samples of 2.5D and 3D C_f/SiC composites on their oxidation rates, the mass change was normalised with respect to the initial (measured prior to oxidation test) mass as:

$$\Delta m \quad (\%) = \frac{m - m_0}{m_0} \times 100 \tag{i}$$

where Δm is the mass change in percentage, m_0 is the initial mass and m is the mass after oxidation.

The as-received composites are referred to as 2.5D C_f/SiC-AR and 3D C_f/SiC-AR in the present study. The composites exposed at 1250 °C are labelled as 2.5D C_f/SiC-1250 °C and 3D C_f/SiC-1250 °C. In a similar manner, the names of other composites have been decided according to the temperature of exposure.

2.3. Characterisation of oxide scale

The microstructures of the as-received 2.5D and 3D C_f/SiC composites were examined using a field emission scanning electron microscope (FESEM; model SUPRA 40, Carl Zeiss NTS GmbH, Oberkochen, Germany) for comparison with the oxidation-tested samples. To observe the multilayered interphase with alternating layers of PyC and SiC at high resolution using transmission electron microscopy (TEM), an electron transparent lamellae was prepared using the focused ion beam technique on a dual beam FIB field emission gun system (Auriga Compact, Carl Zeiss, Germany). These samples were subsequently examined using a high-resolution TEM (JEM2100-F HRTEM) operated at an accelerating voltage of 200 kV. Both bright field and dark field imaging modes were utilised to observe and record the fine microstructural details as well as the fibre–matrix interfaces in the C_f/SiC composites, while the constituent phases were identified through selected area electron diffraction (SAED) analysis.

The phases present in the oxide scales of cyclic oxidation tested samples were identified by XRD analysis (Bruker D8 Advance). The microstructures of the oxide scale top surfaces and cross-sections were examined using a FESEM (model SUPRA 40 FESEM, Carl Zeiss NTS GmbH, Oberkochen, Germany) operated at 20 kV in secondary electron (SE) and backscattered electron (BSE) imaging modes. Furthermore, the chemical compositions from various locations of the microstructures were determined using point analysis and mapping modes of energy dispersive spectroscopy (EDS) facility (model 7425, Oxford Instruments, Wycombe, UK) attached to the FESEM. Additionally, the presence of boron in the oxide scale as well as within the cross-sectional microstructures was qualitatively confirmed using a ToF-SIMS (model PHI nano TOF II, ULVAC-PHI. ING). For the ToF-SIMS analysis, Bi^+ was used as the primary ion source, and Ar^+ was used for sputtering. Using the ToF-SIMS, the acquisition of spectra as well as mosaic mapping were carried out over an area of 200 × 200 μm^2. Additionally, to obtain the 3D composition of oxide scales, depth profiling of both the oxide scale surface and cross-section was carried out by Ar^+ ion sputtering.

2.4. Evaluation of post-oxidation strength retention

The post-oxidation retained strength was measured using a three-point bend test on the oxidation-tested samples of 2.5D C_f/SiC and 3D C_f/SiC composites using a universal testing machine (INSTRON 3365) following the procedure described in ASTM C1341–13 standard [40]. The 2.5D C_f/SiC composite samples having the dimensions of

75 mm× 12 mm× 3.5 mm were subjected to flexural tests at a crosshead velocity of 10.2 mm/min using a three-point bend fixture with a span length of 64 mm. On the other hand, the 3D C_f/SiC composite samples having the dimensions of 105 mm× 17 mm× 5.5 mm were three-point bend tested using a span length of 96 mm at a crosshead velocity of 15.6 mm/min. The dimensions of the test samples were determined based on the thickness of the CVI processed 2.5D and 3D composite panels (mentioned in Section 2.1). Since 3D C_f/SiC composites were fabricated with a higher thickness due to the structural configuration of their fibre preforms, the corresponding test samples and crosshead velocity were proportionally larger according to the specifications outlined in the ASTM C1341–13 standard, to reduce the impact of difference in the sample size [40]. In order to understand the mechanism of fracture, the fracture surfaces of the flexural test samples were examined using the FESEM.

3. Results

3.1. Microstructure

The FESEM (BSE) images along with the characteristic X-ray spectrum and elemental maps obtained by EDS analysis of the cross-section providing information about the structure and chemical composition of carbon fibre bundles, fibre-matrix interphase, SiC/Si-B-C matrix and SiC seal-coating in 2.5D C_f/SiC and 3D C_f/SiC composites, are shown in Fig. 1. Carbon fibres, with a diameter of ~6.4 ± 0.8 μm have significantly different orientations in these composites, as depicted in Fig. 1(a) and (b). In the 2.5D C_f/SiC composite, the carbon fibres are primarily aligned along the x- and y-directions (Fig. 1(a)), whereas in the 3D C_f/SiC composite, they are aligned along three mutually orthogonal directions (Fig. 1(b)). The details regarding the microstructures of these composites have been already reported in an earlier study by the author [29]. The cross-section of the composites, as depicted in Fig. 1(c) and (d), highlights the presence of a CVD SiC seal coating along the edges, as well as a Si-B-C layer embedded within the SiC matrix of both 2.5D C_f/SiC and 3D C_f/SiC composites, respectively. The Si-B-C layer is primarily located in the matrix between the carbon fibre bundles with a thickness of ~7 ± 0.9 μm, while the CVD SiC coating at the composite surface exhibits a thickness of ~26 ± 4 μm. Furthermore, the multilayered interphase with alternating layers of PyC and SiC (with a thickness of 0.16 ± 0.04 μm) around the carbon fibre, is depicted at a higher magnification in the FESEM image shown in Fig. 1(e). A bright field TEM image showing the carbon fibre and a layer of PyC and SiC interphase, along with the SAED patterns from the respective phases, is shown in Fig. 1(f). The PyC layer has been found to have a thickness of ~51 ± 10 nm and the corresponding SAED pattern from the PyC layer exhibits multiple diffraction rings confirming its polycrystalline nature. Furthermore, the SAED pattern from the carbon fibre in Fig. 1(f) is

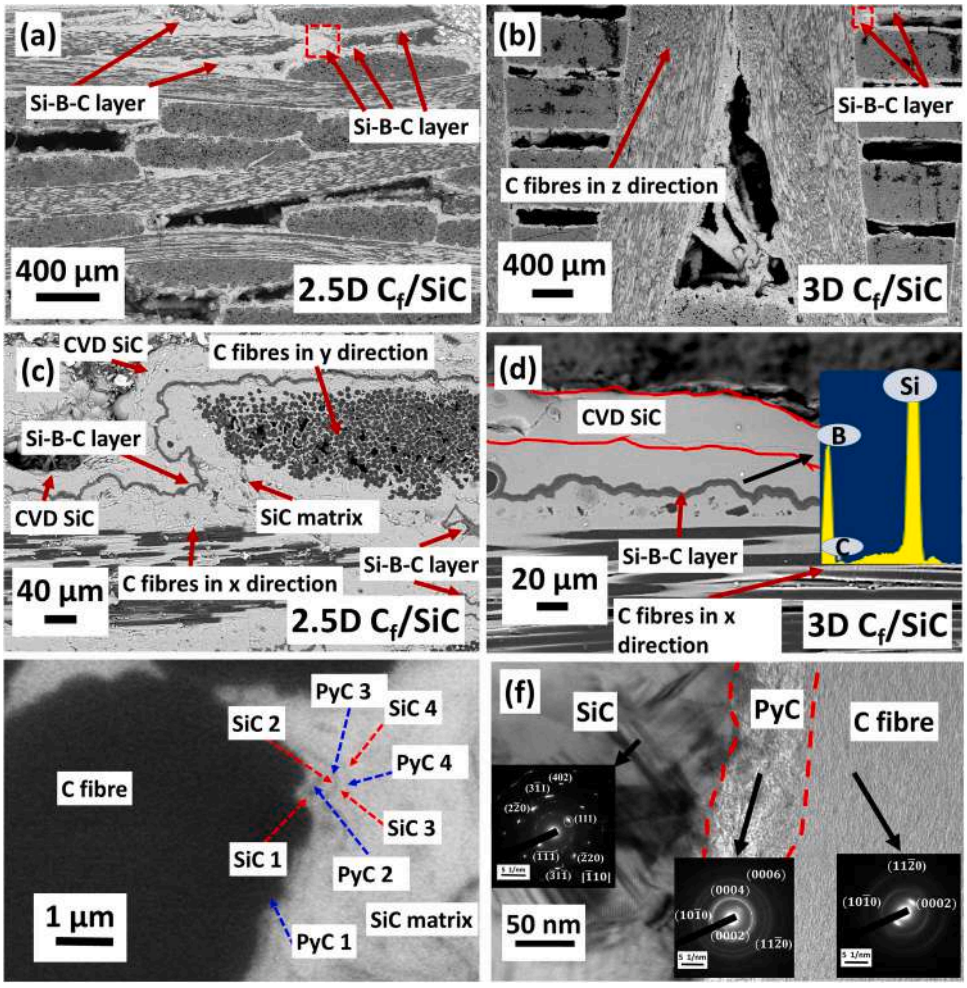

Fig. 1. FESEM (BSE) images depicting the cross-sectional microstructure of (a) 2.5D and (b) 3D C_f/SiC composites at a low magnification, as well as CVD SiC and Si-B-C layer in (c) 2.5D and (d) 3D C_f/SiC composites at high magnification, along with (e) the $(PyC/SiC)_{n=4}$ interphase with alternating layers of PyC and SiC around carbon fibre in the 2.5D C_f/SiC composite and as well as (f) a bright field TEM image of the interphase showing the sequentially arranged layers of PyC and SiC adjacent to the carbon fibre in the 2.5D Cf/SiC with the corresponding SAED patterns from each of the phases in insets. The red squares marked on Si-B-C layer in (a) and (b) indicate typical locations examined by ToF-SIMS depth-profiling (Figs. 12 and 13).

characterised by a pair of arcs, which is indicative of a basal (0002) texture, i.e. preferred orientation of the basal plane along fibre axis. On the other hand, the SAED pattern from the SiC interphase, upon indexing, confirms the presence of β-SiC grains.

Both FESEM and TEM images of the cross-sectional microstructures depicting various layers of the interphase, have been already illustrated in a couple of earlier publications by the authors [29,38].

For the present study, the 2.5D and 3D carbon fibre preform panels were fabricated with carbon fibre volume fractions of 40 % and 36 %, respectively. The volume fractions of carbon fibres in x-, y- and z-directions of 2.5D and 3D C_f/SiC composites along with inter-fibre and inter-bundle porosity measured using X-ray micro CT are listed in Table 1. The approach used to calculate the approximate volume fraction of carbon fibres in each direction of the C_f/SiC composites are described in the previous work by the authors [29]. The results in Table 1 lead to the following inferences: (i) the volume fraction of carbon fibres in z-direction is significantly higher by two orders of magnitude in the 3D C_f/SiC composites; (ii) the 3D C_f/SiC composites exhibit fivefold higher inter-fibre porosity than the 2.5D composites, suggesting more voids between individual fibres; whereas (iii) the inter-bundle porosity in the 2.5D C_f/SiC composites is greater compared to the 3D C_f/SiC composites by a factor of 1.3.

3.2. Non-isothermal oxidation

The TGA generated plots of mass change against temperature for both 2.5D and 3D C_f/SiC composites, as depicted in Fig. 2, show no observable change in mass till ~400 °C followed by a relatively minor mass loss till 600 °C. On increasing the temperature beyond 600 °C, a significant mass loss is observed, which is ascribed to the rapid oxidation of carbon fibres. The plotted data in Fig. 2 indicate that the mass loss in 2.5D C_f/SiC composite is arrested and is followed by a minor gain at ~1100 °C, probably due to the oxidation of SiC to form SiO_2. On the other hand, the mass loss is continued in the 3D C_f/SiC composite at temperatures > 1000 °C, but at a noticeably reduced rate. Both the minor mass gain in the 2.5D C_f/SiC composite as well as the reduced rate of mass loss in the 3D C_f/SiC composite are ascribed to the mass gain by the profuse formation of SiO_2 through the oxidation of SiC at temperatures > 1000 °C.

3.3. Cyclic oxidation

3.3.1. Mass change

Plots showing the variation of mass change with time for 2.5D and 3D C_f/SiC composites subjected to cyclic exposure for 100 h at 1250 °C, 1400 °C and 1500 °C are shown in Fig. 3(a-c). From Fig. 3(a-c), it can be concluded that the 3D C_f/SiC composite samples have exhibited more mass loss than the 2.5D C_f/SiC composite at all the test temperatures. Based on the plot shown in Fig. 3(a), the mass loss of the 2.5D C_f/SiC composite is rapid during the first 10 h of exposure at 1250 °C, and then it continues at a relatively reduced rate following an almost linear

Table 1
Volume fraction of carbon fibres in x-, y- and z-directions, inter fibre porosity and inter-bundle porosity.

Sample	Volume fraction of carbon fibre in x-direction (%)	Volume fraction of carbon fibres in y-direction (%)	Volume fraction of carbon fibres in z-direction (%)	Inter-fibre porosity (%)	Inter-bundle porosity (%)
2.5D C_f/SiC	19.94	19.94	0.12	0.8	8
3D C_f/SiC	10.9	10.9	13.9	4.1	6

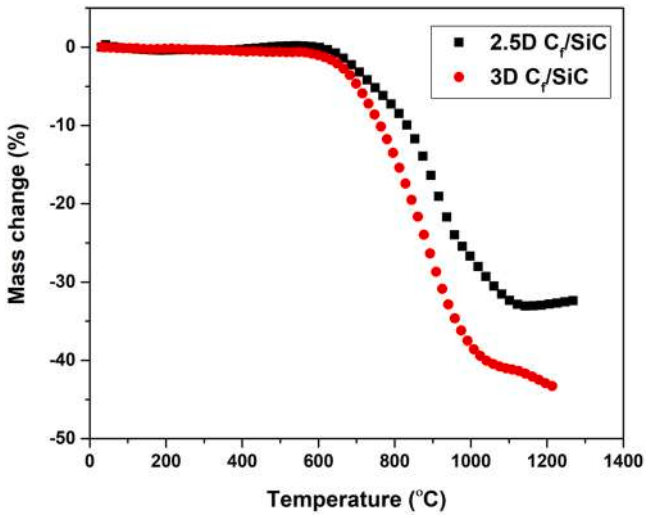

Fig. 2. Plots showing the variation of mass change with temperature for 2.5D and 3D C_f/SiC composites during heating in air up to ~1250 °C at the rate of 10 °C/min inside a TGA.

relationship with the time of exposure. On the contrary, a negligible change in mass has been recorded during the cyclic exposure for 100 h at 1400 °C (Fig. 3(b)). At 1500 °C, the mass loss recorded for the 2.5D C_f/SiC composites decreases steadily as shown in Fig. 3(c). Contrary to the 2.5D C_f/SiC composite, the mass loss behaviour of the 3D C_f/SiC composite follows a more or less similar trend at all three test temperatures, where the rate is gradual in the initial stage of exposure and increases exponentially after ~60 h. Furthermore, the bar charts depicted in Fig. 3 (d) lead to the following inferences: (i) the 2.5D C_f/SiC composite samples exposed at 1400 °C have exhibited a lower mass loss compared to 1250 and 1500 °C; (ii) at each test temperature, the net mass loss of the 3D C_f/SiC composite is greater by an order of magnitude compared to the 2.5D C_f/SiC composite; and (iii) the 3D C_f/SiC composite has exhibited the highest mass loss (~26 %) on exposure at 1250 °C.

3.3.2. Identification of phases from the oxide scale and cross-section

The XRD patterns obtained from the surface and cross-section of the oxide scales formed on 2.5D and 3D C_f/SiC composites subjected to cyclic exposure at 1250 °C, 1400 °C and 1500 °C for 100 h are shown in Fig. 4. The XRD patterns of the as-received 2.5D and 3D C_f/SiC composite samples are also included, in Fig. 4 for the purpose of comparison. The XRD patterns obtained from the surfaces of oxide scales (Fig. 4(a) and (b)) formed by cyclic exposure show the peaks of crystalline SiO_2 (cristobalite). The intensities of XRD peaks representing the SiO_2 is found to be the highest for the samples exposed at 1400 °C for both 2.5D and 3D C_f/SiC composites, as shown in Fig. 4(a) and (b), respectively. Additionally, the XRD patterns from the oxide scale top surfaces as well as cross-sections of the C_f/SiC composites show peaks indicating the presence of highly textured β-SiC (111). Based on the XRD data, it is therefore inferred that the < 111 > is the preferred orientation of the SiC seal coating grown through CVD. The observed decrease in the intensity of SiC (111) peaks after cyclic exposure for 100 h is ascribed to the oxidation of SiC present in the seal coating and matrix of the composites.

The XRD data obtained from the cross-section of oxide scales formed on 2.5D (Fig. 4(c)) and 3D C_f/SiC (Fig. 4(d)) composites confirm the penetration of oxygen well underneath the outer SiC seal coating, causing varying degrees of partial internal oxidation depending on the test temperature. On examining Fig. 4(c) and (d), it is noted that in comparison to the as-received composite samples, the XRD peak intensities from the basal plane (0002) of carbon obtained from the samples subjected to cyclic oxidation tests are considerably lower or

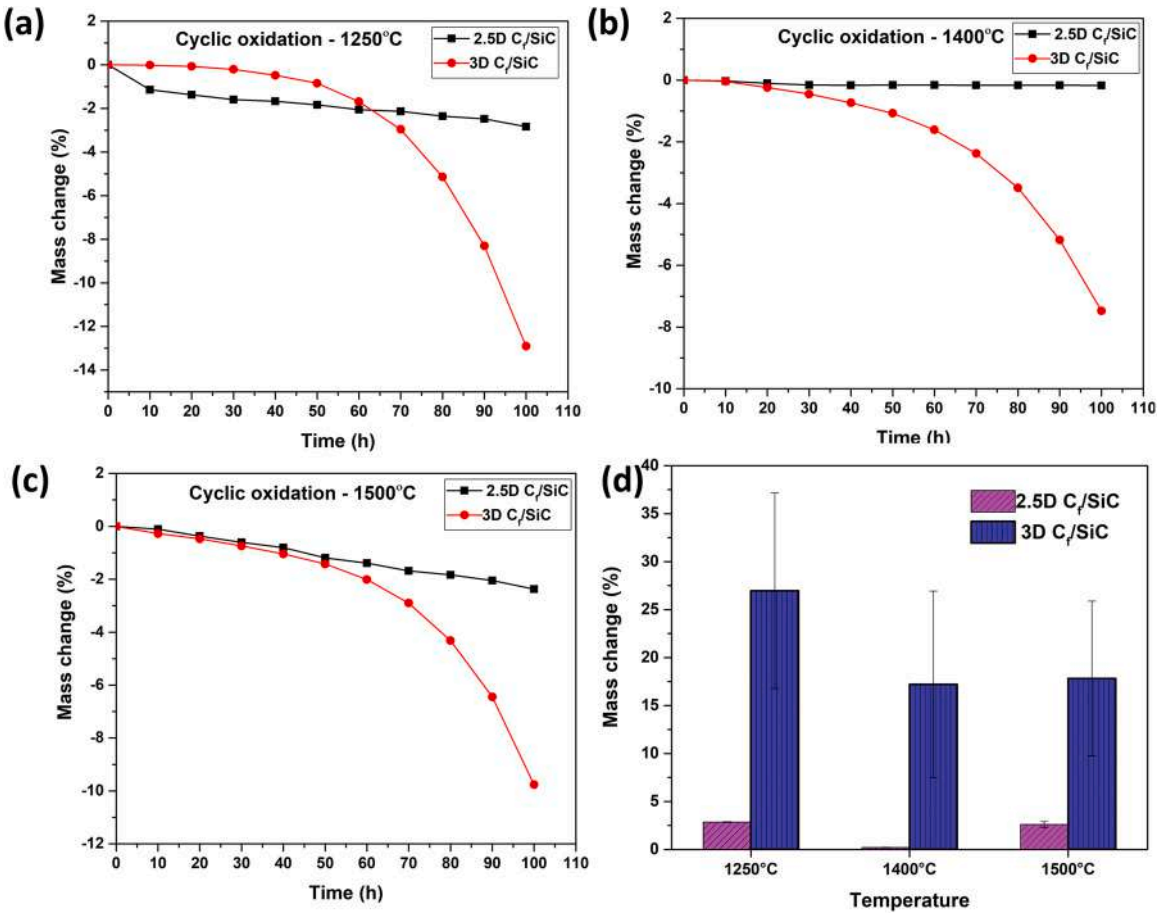

Fig. 3. Plots depicting the variation of mass change with time for 2.5D and 3D C_f/SiC composites during cyclic exposure at (a)1250 °C, (b) 1400 °C and (c)1500 °C, as well as (d) bar charts depicting the net mass change on exposure for 100 h at these temperatures.

insignificant, indicating that a large fraction of the carbon fibres beneath the oxide scale have been oxidized. Furthermore, a comparison of the (0002) carbon peaks in the XRD patterns from the cyclic oxidation tested 2.5D C_f/SiC and 3D C_f/SiC composite samples which are shown as inset in Fig. 4(c), indicates a steady decrease in their intensity with increase in test temperature from 1250 to 1500 °C. Such a trend is well-expected considering that the amount of carbon fibre oxidation would scale with temperature. Interestingly, as shown in Fig. 4(d) and its inset, the broad peak representing the (0002) basal plane of carbon is absent in the XRD pattern from the 3D C_f/SiC-1250 °C composite, which indicates that a significant amount of carbon fibres have been most severely oxidised. Nevertheless, the broad peaks of carbon (0002) basal plane can be found at 26.13° in the XRD pattern from the oxide scale of the 3D C_f/SiC composite sample exposed at either 1400 °C or 1500 °C. The presence of (0002) carbon peaks in the XRD patterns of oxide scales formed on 2.5D C_f/SiC composites exposed at 1250 °C, 1400 °C and 1500 °C as well as the 3D C_f/SiC composites exposed at 1400 °C and 1500 °C, indicates that the carbon fibres in these composites retain their structural integrity even after a prolonged exposure of 100 h at the aforementioned temperatures. From the XRD results shown in Fig. 4, it is concluded that the SiO_2 scale formed at the surfaces of 2.5D and 3D C_f/SiC composites at the above-mentioned specific temperatures is more or less protective in nature, and thereby shields the underneath substrate from further oxidation.

3.3.3. *Microstructural analysis of composites after cyclic exposure*

The surface morphologies of the oxide scales formed on 2.5D and 3D C_f/SiC composites exposed to cyclic oxidation, are illustrated with the help of FESEM (SE) images in Fig. 5. For the 2.5D C_f/SiC composites (Fig. 5(a) to (c)), the oxide scale morphologies appear to vary quite sharply from one another, depending on the temperature of exposure during cyclic oxidation. For example, the oxide scales formed on 2.5D C_f/SiC composite exposed at 1250 °C and 1400 °C (Fig. 5(a) and (b)) are constituted by globular clusters of grains, having a typical cauliflower-like appearance. On the contrary, the surface of the oxide scale formed on exposure at 1500 °C appears relatively smooth and uniform in comparison to those formed at lower temperatures. Furthermore, the edges of the cracks formed in the oxide scale during cyclic exposure at 1250 °C (Fig. 5(a) inset) appear to be filled with silica/borosilicate glass. However, the oxide scale formed at 1500 °C appears uniform, covering the granular SiC seal coating (Fig. 5(c)). The formation of cracks on the oxide scales may be ascribed to the internal stresses caused during the repeated cycles (10 times) of heating and cooling due to the mismatch between the thermal expansion coefficients of the SiO_2 scale and SiC underneath it. The oxide scale morphology of the 3D C_f/SiC composite cyclically exposed at 1250 °C as shown in Fig. 5(d), vividly exhibits evidence of a significant amount of spallation, thereby differing significantly from the continuous layer of oxide formed on the 2.5D C_f/SiC composite. On the other hand, a reasonably uniform oxide scale without any evidence of spallation can be seen on the surfaces of oxide scales formed on the 3D C_f/SiC composites through cyclic exposure at 1400 °C and 1500 °C (Fig. 5(e) and (f)) as also highlighted in the insets of these figures.

The FESEM (BSE) images illustrating the cross-sections of the composites subjected to cyclic oxidation are shown in Fig. 6. In the case of the 2.5D C_f/SiC composites (Fig. 6(a-c)), the amount of oxidation-caused damage in the carbon fibres has been found to be insignificant. However, the FESEM (BSE) images depicting the cross sections of samples

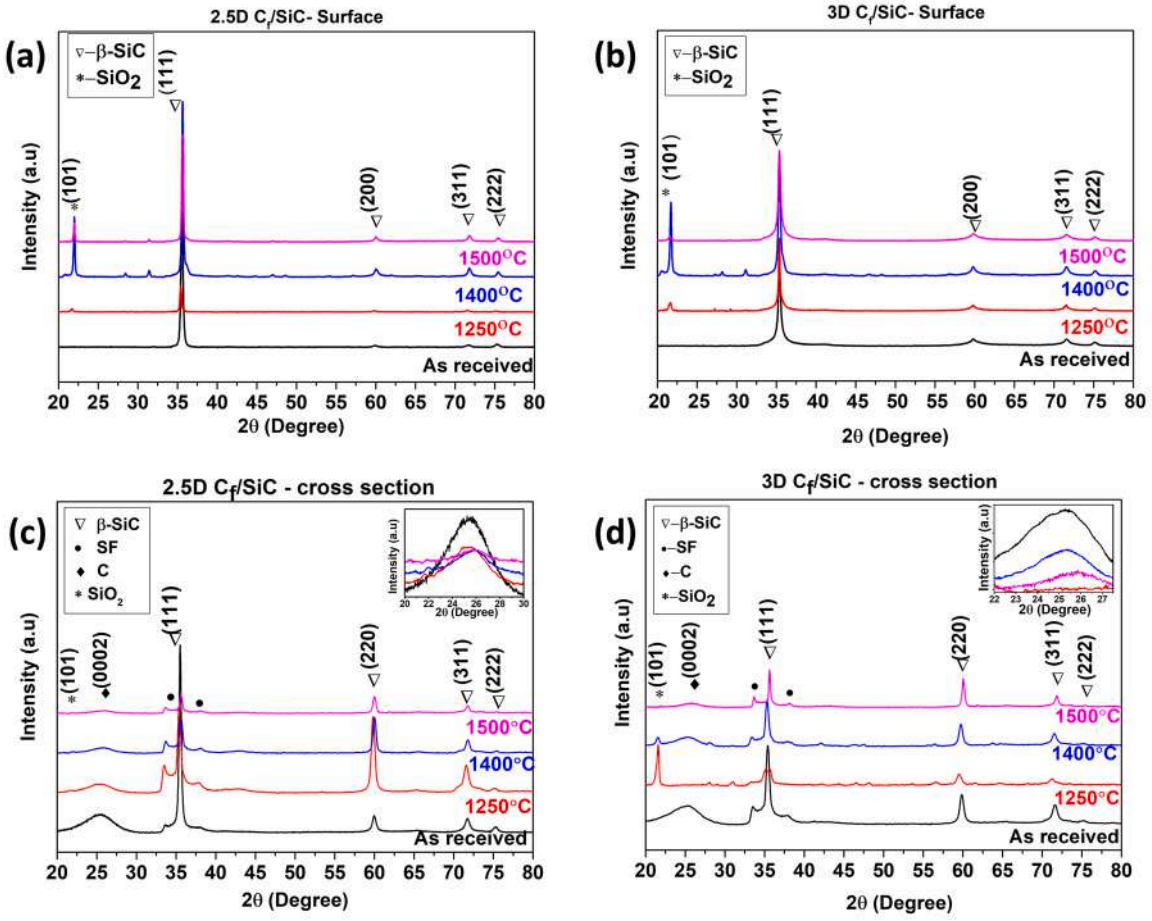

Fig. 4. XRD patterns obtained from the oxide scale top surfaces of: (a) 2.5D and (b) 3D C_f/SiC composites and oxide scale cross-sections of (c) 2.5D and (d) 3D C_f/SiC composites subjected to cyclic exposure for 100 h at 1250 °C, 1400 °C and 1500 °C.

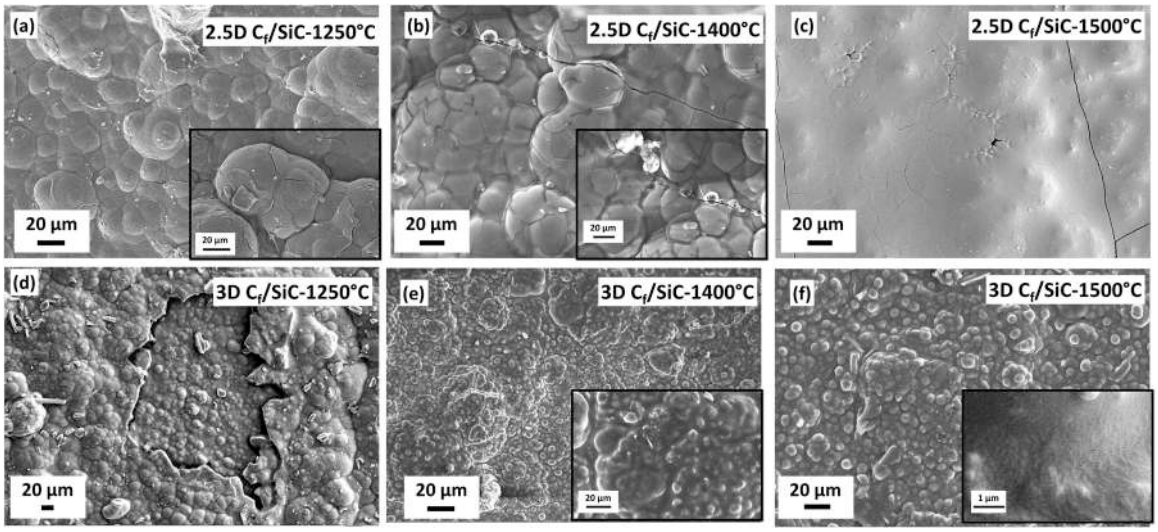

Fig. 5. FESEM (SE) images depicting the surface morphologies of the oxide scales formed on 2.5D and 3D C_f/SiC composites, respectively, after a cyclic exposure for 100 h at: (a and d) 1250 °C, (b and e) 1400 °C and (c and f) 1500 °C.

cyclically exposed at 1500 °C (Fig. 6(c)) show the presence of cavities in the matrix (marked in red ellipses), which probably have originated from the escape of SiO (g) formed by the active oxidation of SiC. Significant degradation of the composites is evident from the locations marked by red ellipses in the SEM (BSE) images, indicating localised oxidation of carbon fibres in the 3D C_f/SiC composites exposed at 1250 °C (Fig. 6(d)). Moreover, a substantial oxidation of carbon fibres is found to have occurred along the z-direction of the 3D C_f/SiC composites, as confirmed by the magnified view of the oxidised surface shown as the inset of Fig. 6(d). In contrast, the oxidation of carbon fibre appears to be

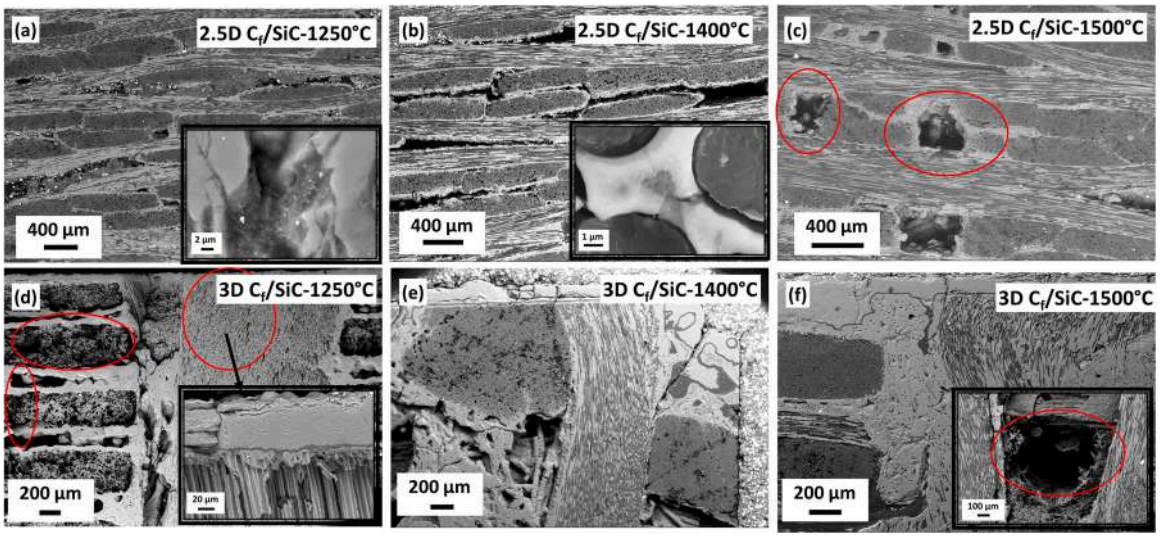

Fig. 6. FESEM (BSE) images depicting the cross-sectional microstructures of the 2.5D and 3D C_f/SiC composites after cyclic exposure for 100 h at: (a and d) 1250 °C, (b and e) 1400 °C, as well as (c and f) 1500 °C. The image in (d) shows the damage caused by oxidation of carbon fibres within red ellipses. The images in (c) and (f) along with the inset in (f) illustrate cavities having sizes in the range of 200–400 µm (inside the red ellipses) caused by localised depletion of the SiC matrix through active oxidation.

significantly limited in the 3D C_f/SiC composites exposed at 1400 °C, as shown in Fig. 6(e). In a manner similar to the 2.5D C_f/SiC exposed at 1500 °C, the matrix of 3D C_f/SiC-1500 °C composite also consists of cavities indicating a somewhat profuse escape of gases formed as oxidation products (discussion on operative mechanisms can be found in Sections 4.1–4.3).

The FESEM images depicting the oxide scale microstructures along with the corresponding EDS spectra depicting the elemental distribution within the oxide scales of 3D C_f/SiC composites are shown in Fig. 7. The region of oxide scale subjected to spallation is indicated in red colour (Fig. 7(a)), and the corresponding EDS spectrum with the peaks of Si, O and B confirms that this location is oxidized and contains borosilicate glass. The SEM image in Fig. 7(b) depicting the oxide scale top surface of the 3D C_f/SiC composite exposed at 1400 °C, shows the presence of relatively fewer defects compared to those found in the oxide scales formed at 1250 and 1500 °C. The borosilicate glass is found to seal the pores present in the oxide scale of the 3D NOOBed composite (marked by the red ellipses) exposed at 1400 °C, as shown in Fig. 7(b). In a similar manner, the formation of a partially continuous scale of borosilicate glass is visible in the cross-section of 3D C_f/SiC composite cyclically exposed at 1500 °C, as shown in Fig. 7(c).

The FESEM (BSE) images along with the corresponding EDS X-ray elemental maps from the cross-section of the oxide scale formed on 2.5D and 3D C_f/SiC composites subjected to cyclic exposure of 100 h at 1400 °C are shown in Fig. 8 and Fig. 9, respectively. Based on the FESEM images and EDS data depicted in Figs. 8 and 9, it is evident that a distinct layer of SiO_2 has formed on the SiC seal coating surfaces of both 2.5D and 3D C_f/SiC composites. The average thickness with standard deviations measured from the SEM (BSE) images of the oxide scale cross-sections (as shown in Figs. 8 and 9, for example) in the composites subjected to cyclic oxidation tests are listed in Table 2, and indicate a noticeable as well as sharp increase between 1250 °C and 1400 °C, but a very minor increase with the increase in the test temperature to 1500 °C. The measured values of oxide scale thickness are considered to be related to the net change in mass, as well as the amount of spallation caused by thermal shock.

3.3.4. Three-dimensional analysis of oxide scale composition using ToF-SIMS depth profiling

A detailed TOF-SIMS study with depth profiling has been performed on the 2.5D C_f/SiC composites subjected to cyclic exposure for 100 h at 1400 °C, and 3D C_f/SiC composites cyclically exposed for the same duration at 1250 °C and 1400 °C. The reasons for selection of these samples are based on the net mass change depicted using bar charts in Fig. 3(d), which lead to the following inferences: (i) for the 2.5D C_f/SiC composite, the minimum mass loss has been observed on cyclic exposure for 100 h at 1400 °C, and (ii) for the 3D C_f/SiC composite, maximum and minimum mass loss has been observed on cyclic exposure at 1250 °C and 1400 °C, respectively. Fig. 10 illustrates the ion images (Fig. 10(a), (d), (g) and (j)) and the corresponding maps of total ions (Fig. 10(b, e, h and k) and BO^- ions (Fig. 10(c), (f), (i) and (l)) obtained using the ToF-SIMS from oxide scales and cross-section of 2.5D C_f/SiC and 3D C_f/SiC composites subjected to cyclic exposure of 100 h at 1400 °C. In the images depicted in Fig. 10, a given colour (varying from yellow to white) indicates the high concentration of a particular type of ions on the scanned surface, while the red colour represents the ions having lower to medium concentration. Based on a qualitative comparison of the colour maps in the images obtained from the oxide scales of the 2.5D and 3D C_f/SiC composites, it is inferred that the amount of BO^- ions at the top surfaces of the oxide scale is substantially greater than that in their cross-sections. The aforementioned observations confirm that the boron has diffused from the Si-B-C layer underneath the SiC seal coating to the surface, which facilitates the formation of an oxide scale containing the borosilicate glass with self-healing property, such that the carbon fibres in the composite are not degraded by oxidation.

The ToF-SIMS depth profiles obtained from the oxide scale and cross-section of 2.5D C_f/SiC-1400 °C (Fig. 11(a) and (b)), 3D C_f/SiC-1400 °C (Fig. 11(c) and (d)) and 3D C_f/SiC-1250 °C (Fig. 11(e) and (f)), have been depicted by plotting the normalised counts of the secondary ions against the sputtering duration. In the plots depicted in Fig. 11, the sputtered depth beneath the surface of the oxide scale is considered to scale with the sputtering duration. An effort to measure the actual depth by a profilometer did not succeed due to the rough surface of the oxide scale.

To estimate the sputtering rate, a thermally grown SiO_2 film on a Si (100) wafer was used as a reference. A limited area (200 µm x 200 µm) of this SiO_2 film was subjected to ToF-SIMS depth profiling by argon ion sputtering, and the resulting crater depth was measured using a stylus profilometer (KLA Instruments, Milpitas, CA, USA, model Alpha-Step D-600). The sputtering rate for SiO_2 has been determined as ~0.33 nm/s, based on which the sputtered depth of the oxide scale is found as ~69 nm for the oxidation-tested samples of both 2.5D and 3D C_f/SiC

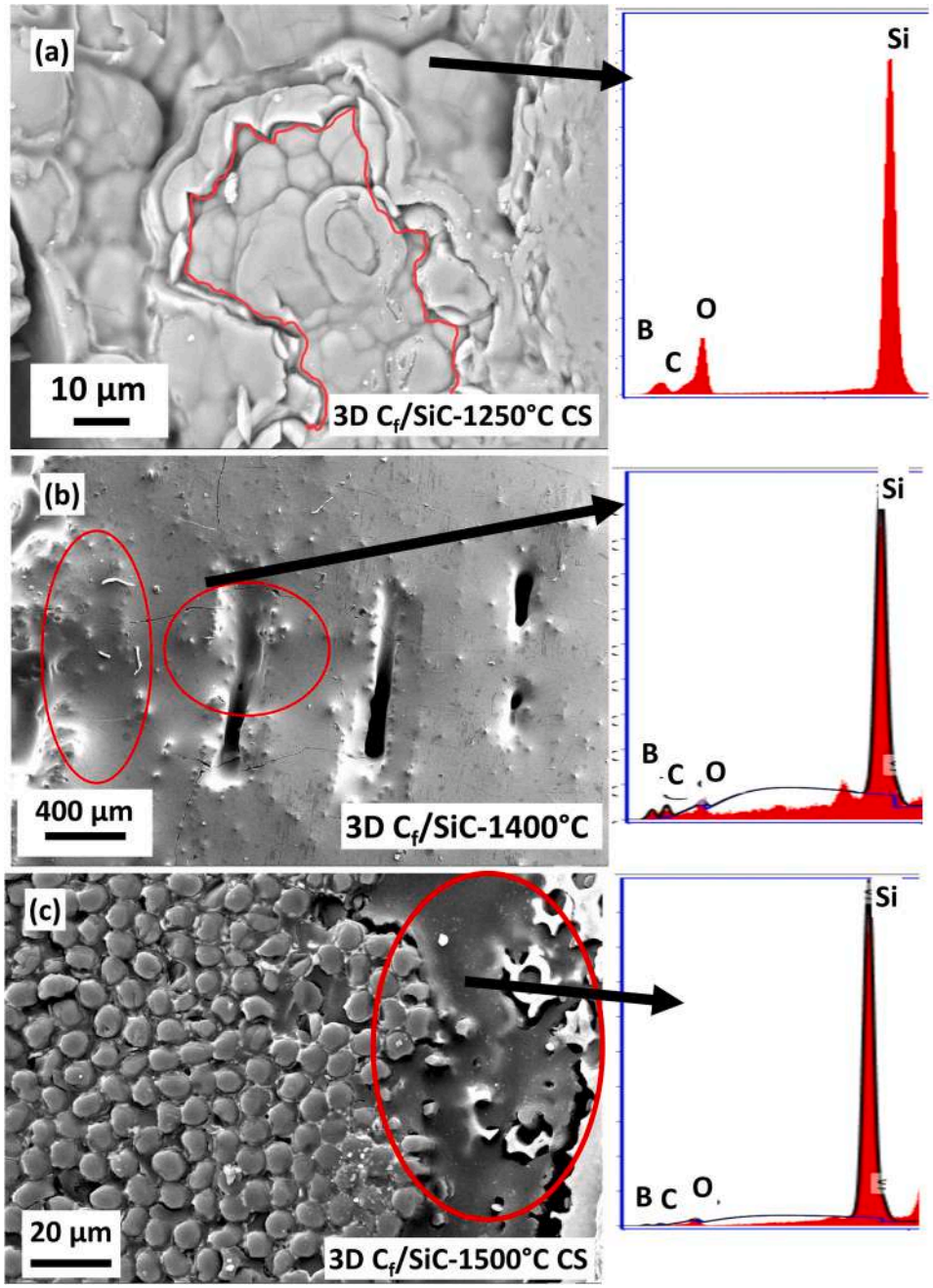

Fig. 7. FESEM images of the oxide scale microstructures and the corresponding EDS spectra showing the peaks of Si, O, B and C, which have been obtained from 3D NOOBed C_f/SiC composite cyclically exposed for 100 h at: (a) 1250 °C, (b) 1400 °C, and (c) 1500 °C. (a) shows evidence of spallation (marked in red); (b) shows inter-bundle pores, some of which appear to be cemented by borosilicate glass (red ellipses); and (c) indicates partial healing by growth of the borosilicate glass (red ellipse).

composites.

For both 2.5D C_f/SiC-1400 °C and 3D C_f/SiC-1400 °C composites, the concentration of O appears to have remained more or less constant within the depth of oxide scales investigated by ToF-SIMS depth profiling, indicating complete oxidation of the SiC/Si-B-C matrix, as shown in Fig. 11(a) and (c). Additionally, the compositional profiles shown in Fig. 11(a) and (c) indicate the presence of boron both at the surfaces as well as throughout the depth of oxide scales formed on 2.5D and 3D C_f/SiC composites exposed at 1400 °C, indicating the formation of a layer of borosilicate glass. The depth profiles from the cross-sections of these composites exposed at 1400 °C (Fig. 11(b) and (d)) indicate that at a given depth, the intensity of oxygen ions from the cross-section is significantly lower than that of Si and C ions. This observation suggests that a protective layer may have formed on the surface, such that the ingress of oxygen into the composite is hindered. On the other hand, the depth profiling carried out on the oxide scale top surface and the cross-section of the 3D C_f/SiC composites exposed at 1250 °C for 100 h (Fig. 11(e) and (f)) indicate that the apparent concentration of oxygen is higher by an order of magnitude compared to that of B or C, which suggests penetration of oxygen to a significant depth along with resultant oxidation and structural degradation.

The 3D ion maps obtained from ToF-SIMS depth profiling (up to 200 or 210 s) of the oxide scale top surface and the cross-section of the 2.5D C_f/SiC composite exposed at 1400 °C and the 3D C_f/SiC composite exposed at 1250 °C are shown in Fig. 12 and Fig. 13, respectively. The cross-sectional region selected for depth profiling (marked in red square

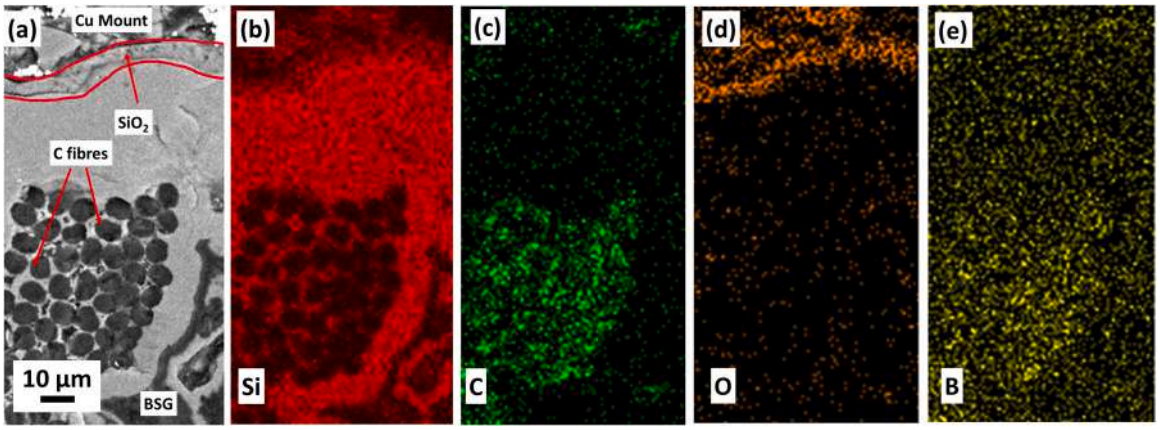

Fig. 8. SEM (BSE) images and the corresponding EDS X-ray maps from the cross-section of the oxide scale formed on the surface of 2.5D C_f/SiC composites subjected to cyclic exposure at 1400 °C.

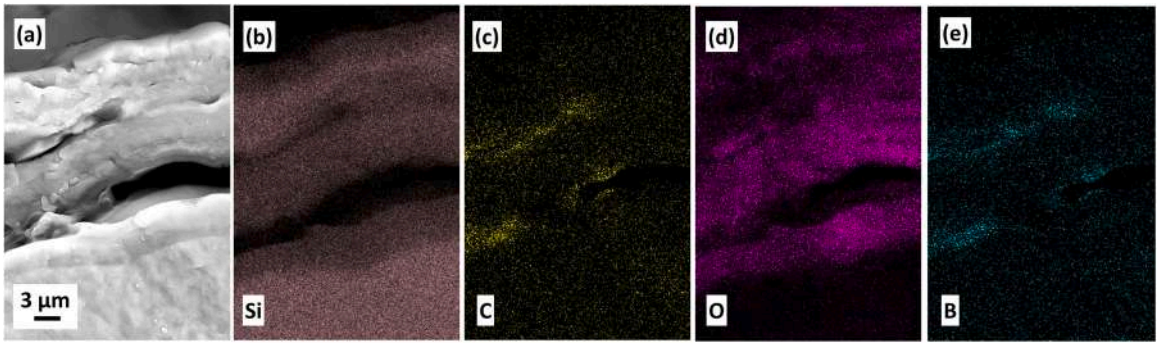

Fig. 9. FESEM (BSE) image and the corresponding EDS X-ray maps depicting the elemental distribution within the cross-section of the oxide scale formed on the surface of 3D C_f/SiC composites subjected to cyclic exposure of 100 h at 1400 °C.

Table 2
Measured values of oxide scale thickness.

Temperature (°C)	Oxide scale thickness (µm)	
	2.5D C_f/SiC	3D C_f/SiC
1250	4.49 ± 1.99	3.2 ± 0.69
1400	5.63 ± 1.69	6.16 ± 1.45
1500	5.9 ± 2.3	6.18 ± 2.16

in Fig. 1(a) and (b)) was located adjacent to the SiBC layer, to analyse the relative amounts of oxygen and boron in comparison to the oxide scale surface. The ions found through the ToF-SIMS depth profiling of the oxide scale top surface (up to 200 or 210 s) on the 2.5D C_f/SiC-1400 °C are BO^-, BO_2^- and SiO^-, which are shown using blue, purple and red colours, respectively in the 3D ion maps depicted in Fig. 12(a) to (e). In a similar manner, the ions obtained by depth profiling of the cross-section are found to be primarily SiC^- (shown as green), as shown in Fig. 12(f) to (j). These observations indicate that the SiC matrix within the cross-section has been protected from oxidation even after a prolonged exposure at 1400 °C.

Fig. 13(a) to (e) depict the 3D ion maps obtained through depth profiling (up to 200 or 210 s) of the oxide scale top surface, whereas Fig. 13(f) to (j) exhibit similar maps obtained from the cross-section of 3D C_f/SiC-1250 °C composite exposed cyclically at 1250 °C for 100 h. From the images shown in Fig. 13, it is noted that the amounts of BO^- and BO_2^- ions present in the cross-section are significantly greater than those at the surface of the oxide scale. Furthermore, the intensity of SiC^- ions is lower in both the oxide scale top surface and cross-section, indicating the formation of SiO_2. The 3D ion maps in Fig. 13 indicate that the sub-surface SiC matrix (analysed by depth profiling up to 200 s) of the 3D C_f/SiC-1250 °C is oxidised, indicating that the SiO_2 formed at the surface is discontinuous, and therefore non-protective.

3.3.5. *Flexural Strength*

Typical flexural stress-strain curves obtained from the three-point bend tests carried out on 2.5D and 3D C_f/SiC composites after 100 h of cyclic oxidation, along with the bar-charts depicting both mean and standard deviation of the flexural strengths are illustrated in Fig. 14. The following inferences can be drawn from the results presented in Fig. 14: (i) all the flexural stress-strain curves depict pseudo-ductile behaviour with the initial elastic part of stress-strain curve appearing linear and the latter part deviating from linearity (Fig. 14(a) and (b)); (ii) the deviation from linearity considered as the characteristics of graceful failure is greater in the stress-strain curves of the oxidation-tested specimens compared to those tested in as-received condition (Fig. 14(a) and (b)); (iii) the flexural strengths of the oxidation-tested 2.5D and 3D C_f/SiC composite samples are less than those obtained for the corresponding as-received specimens by amounts varying from 18 % to 43 % (Fig. 14(c)); (iv) the standard deviation of the post-oxidation flexural strengths, as well as the reduction compared to the flexural strengths of as-received samples are consistently greater for the 3D C_f/SiC composite specimens than the 2.5D C_f/SiC composite, irrespective of the test temperature (Fig. 14(c)); and (v) the reduction of flexural strength is the least on cyclic exposure at 1400 °C for both 2.5D (~18 %) and 3D C_f/SiC composites (~20 %); whereas (vi) the maximum reduction of flexural strength has occurred on cyclic exposure at different temperatures, 1500 °C (~35 % reduction) for the 2.5D C_f/SiC composite and 1250 °C (~43 % reduction) for the 3D C_f/SiC composite (Fig. 14c).

The FESEM images depicting the morphology of the surface that

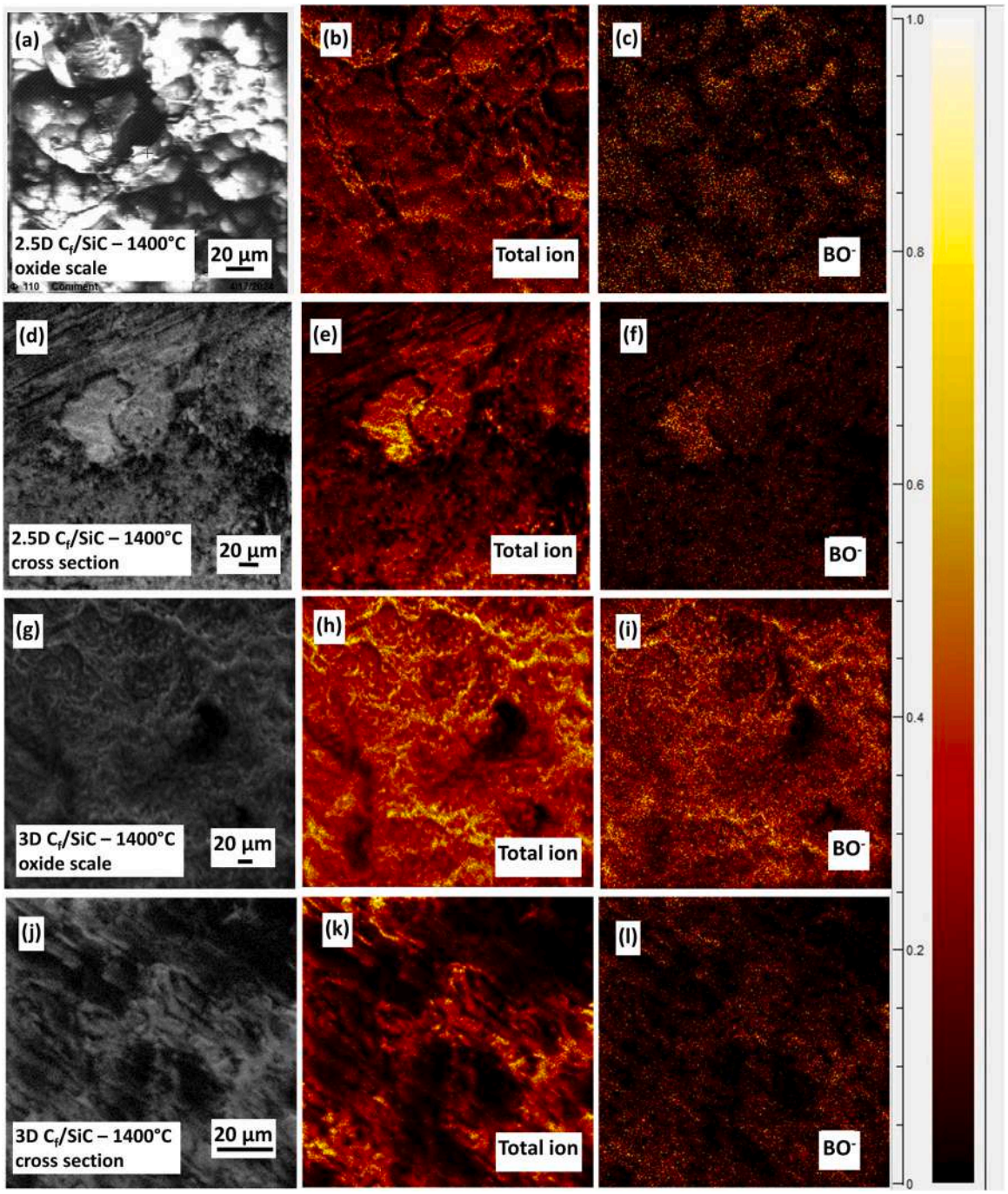

Fig. 10. Ion images as well as the corresponding maps of total ions and BO^- ions obtained using the ToF-SIMS from the oxide scales and cross-section of the C_f/SiC composites exposed cyclically at 1400 °C.

experienced the maximum tensile stress during the three-point bend tests carried out on the oxidation-tested samples of 2.5D and 3D C_f/SiC composites are shown in Figs. 15 and 16, respectively. For both 2.5D and 3D C_f/SiC composites (Fig. 15(b) and Fig. 16(a)), the crack paths in the samples exposed at 1400 °C (indicated by arrows) are found to be more tortuous compared to those observed after cyclic oxidation tests at other test temperatures. Also, it can be noted that the extent of fibre pull-out is higher in the composites cyclically exposed at 1400 °C and 1500 °C (Fig. 15(c) and Fig. 16(b)), which is perfectly in tune with the trend of flexure strain observed in Fig. 14(a) and (b). Another significant observation in the matrix of composites subjected to cyclic exposure at 1500 °C, is the presence of cavities, as indicated by the red ellipse in Fig. 15(c), which may have formed by localised active oxidation of the SiC matrix. From the aforementioned results and fractography, it can be concluded that the C_f/SiC composites exposed at 1400 °C show a higher amount of strength retention and damage tolerance than those expected at other temperatures.

4. Discussion

4.1. Possible chemical reactions involved in oxidation

The possible chemical reactions involved in the formation of oxide scales of the C_f/SiC composites with multilayered interphase and modified matrix, during cyclic exposure for 100 h at 1250 °C, 1400 °C and 1500 °C are listed as follows:

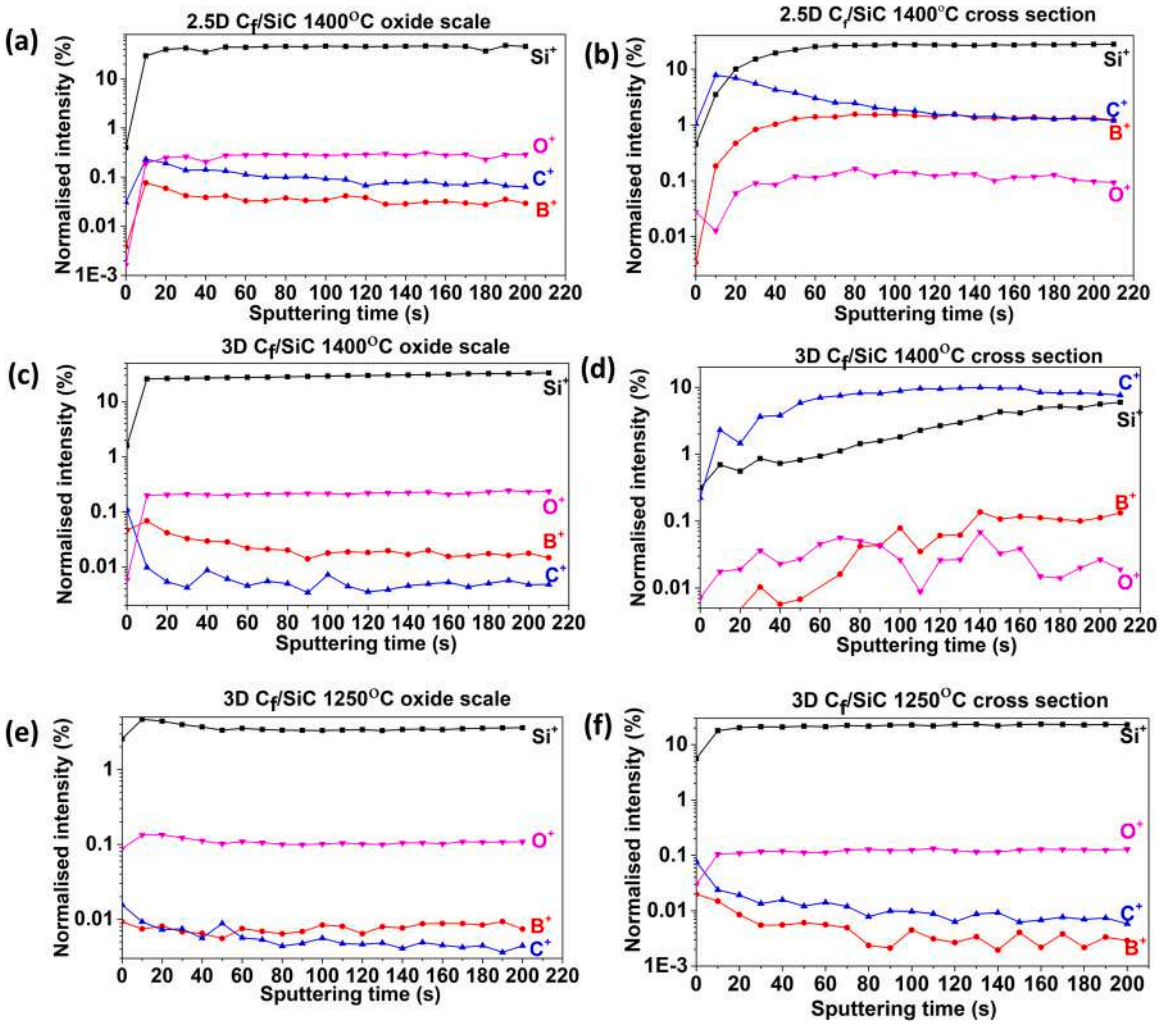

Fig. 11. Depth profiles obtained by using Ar^+ ion sputtering during ToF-SIMS studies on (a) oxide scale (top surface) and (b) cross-section of the 2.5D C_f/SiC composites exposed to cyclic exposure of 100 h at 1400 °C; (c) oxide scale (top surface) and (d) cross-section of the 3D C_f/SiC composites exposed to cyclic exposure of 100 h at 1400 °C; (e) oxide scale (top surface) and (f) cross-section of the 3D C_f/SiC composites exposed to cyclic exposure of 1250 °C for 100 h.

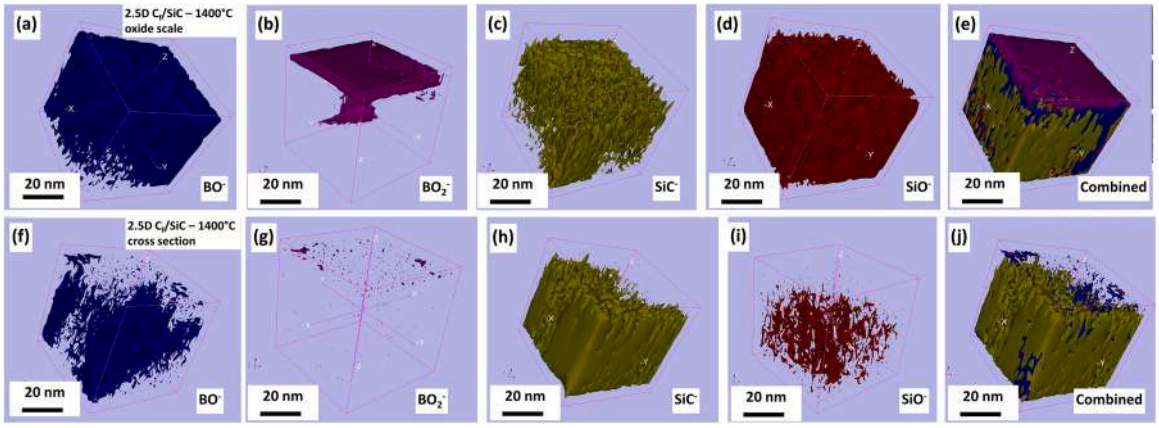

Fig. 12. The 3D ion maps obtained using ToF-SIMS depth profiling on the oxide scale (top surface) of the 2.5D C_f/SiC composite exposed cyclically at 1400 °C for 100 h showing the presence of (a) BO^- (blue), (b) BO_2^- (purple), (c) SiC^- (green), (d) SiO^- (red) and (e) all these ions combined, as well as from the cross-section of the 2.5D C_f/SiC composite (typical location marked with red square in Fig. 1(a)) showing (f) BO^-, (g) BO_2^-, (h) SiC^-, (i) SiO^- and (j) all these ions combined.

$$2SiC\ (s) + 3O_2\ (g) \rightarrow 2SiO_2\ (s) + 2CO\ (g) \quad (1)$$

$$2B_4C\ (s) + 7O_2\ (g) \rightarrow 4B_2O_3\ (l) + 2CO\ (g) \quad (2)$$

$$2C\ (s) + O_2\ (g) \rightarrow 2CO\ (g) \quad (3)$$

$$B_2O_3\ (l) + x.SiO_2\ (l) \rightarrow B_2O_3.x.SiO_2\ (l) \quad (4)$$

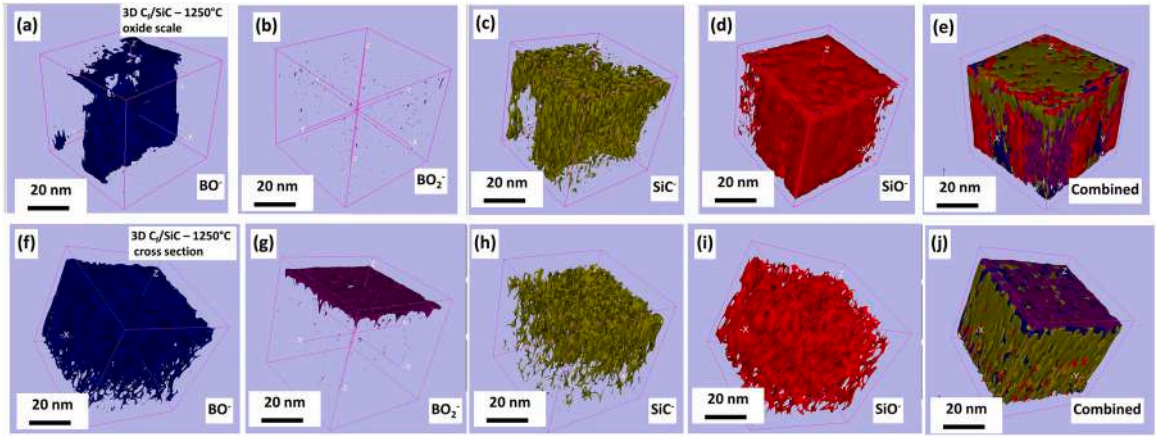

Fig. 13. The 3D ion maps obtained by ToF-SIMS depth profiling at the oxide scale top surface of 3D C_f/SiC composites exposed cyclically at 1250 °C for 100 h showing the enrichment of (a) BO^- (blue), (b) BO_2 (purple), (c) SiC^- (green), (d) SiO^- (red) and (e) all these ions combined, as well as from the cross-section ((typical location marked with red square in Fig. 1(b)) showing (f) BO^-, (g) BO_2, (h) SiC^-, (i) SiO^- and (j) all these ions combined.

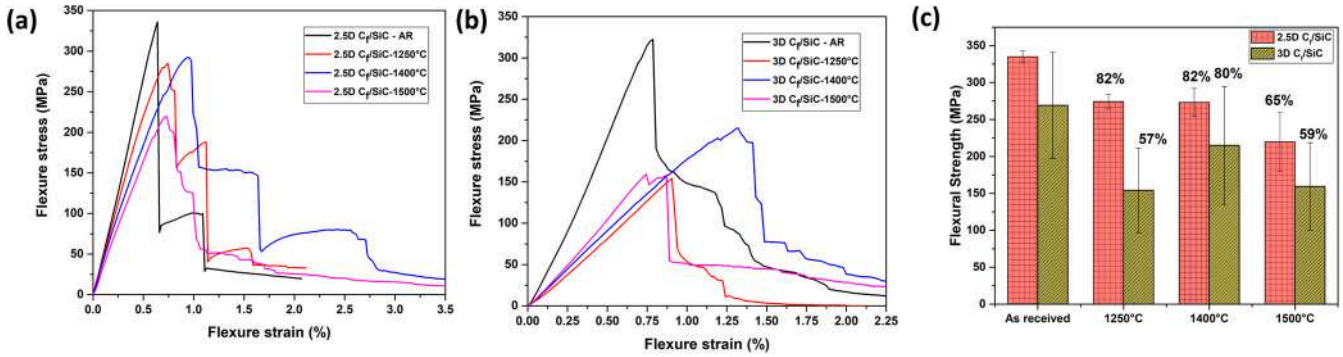

Fig. 14. Flexural stress-strain plots obtained by three-point bend tests on (a) 2.5D C_f/SiC, (b) 3D C_f/SiC composites in as-received conditions and after cyclic exposure at 1250, 1400 and 1500 °C, as well as (c) the bar charts depicting flexural strengths of the investigated C_f/SiC composites.

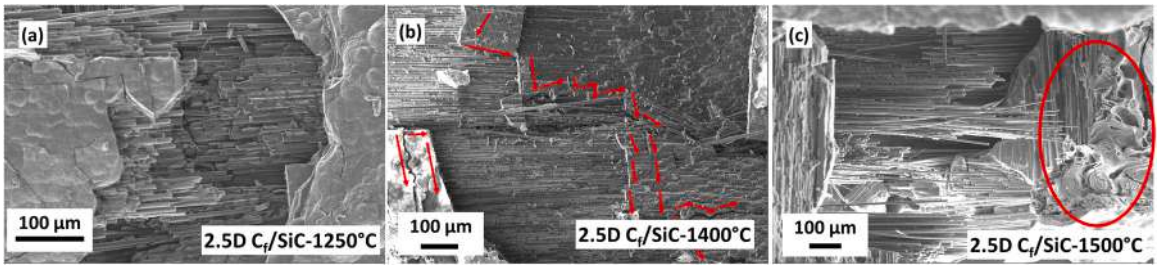

Fig. 15. FESEM images depicting the surfaces of 2.5D C_f/SiC composites under maximum tensile stress during three-point bend tests till failure after cyclic exposure for 100 h, at (a) 1250 °C showing the fibre pull-out, (b) 1400 °C illustrating the crack tortuosity in red arrows and (c) 1500 °C showing the degradation of matrix due to active oxidation (red ellipse).

$$B_2O_3.x.SiO_2\ (l) \rightarrow B_2O_3\ (g) + x.SiO_2\ (l) \quad (5)$$

Additionally, the SiC is known to undergo active oxidation at temperatures $\geq$ 1500 °C through the chemical reaction:

$$SiC\ (s) + O_2\ (g) \rightarrow SiO\ (g) + CO\ (g) \quad (6)$$

Out of the chemical equations listed above, the Reactions (1) and (2) are expected to cause an increase in mass by producing SiO_2 (s) and B_2O_3 (l) as well as mass loss by producing CO (g) during the cyclic oxidation tests on either 2.5D or 3D C_f/SiC composite. However, the Reactions (3) and (6) are expected to generate gaseous products such as CO (g) and SiO (g), having the tendency to escape into the atmosphere through cracks and pores, resulting only in loss of mass. Oxidation by Reactions (3) and (6) are therefore considered to have a detrimental effect on the composites in terms of their strength as well. On the other hand, Reaction (4) leads to the formation of a borosilicate glass layer, which serves as a strong diffusion barrier for the inward penetration of the oxygen from air. Therefore, the formation of borosilicate glass (B_2O_3-SiO_2) is considered advantageous for creating a continuous and protective oxide scale to hinder the subsequent ingress of oxygen. An additional advantage of the borosilicate glass containing oxide scale is its self-healing ability. The presence of B_2O_3 (l) in the borosilicate glass contributes to its plasticity and flowability, which is responsible for its ability to heal cracks and pores in the oxide scale. Although the reduction of viscosity with an increase in B_2O_3 (l) content can increase the plasticity of the scale, it may turn out to be detrimental for permitting greater diffusion

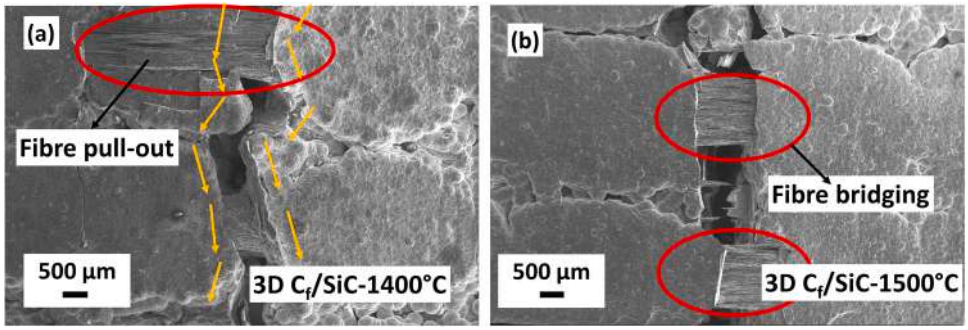

Fig. 16. FESEM images depicting the surfaces of 3D C_f/SiC composites under maximum tensile stress during three-point bend tests till failure after cyclic exposure for 100 h at: (a) 1400 °C, showing fibre pull-out (red ellipse) and deflections in crack path (yellow arrows); and (b) 1500 °C, illustrating fibre pull-out and bridging (within the red ellipses).

of oxygen. However, the amount of B_2O_3 (l) in the borosilicate glass is expected to be depleted by vaporisation through Reaction (5) at the test temperatures (1250, 1400 and 1500 °C), leaving behind a more viscous SiO_2-rich scale, which would be less permeable for oxygen [41]. The oxide scales with silica-rich borosilicate layer have been reported to be stable up to 1700 °C [42], in spite of the vaporisation of B_2O_3 at the test temperatures (1250 °C-1500 °C) leading to mass loss [13,43].

4.2. Thermodynamic feasibility of the oxidation reactions

The thermodynamic feasibility of the chemical reactions (1), (2), (3) and (6) has been analysed by calculating the free energy change per mole of oxygen from the data available in the literature [44]. The thermodynamic stability of the oxides at the investigated temperature is found to increase in the following order: B_2O_3>SiO_2>CO>SiO>CO_2, as shown in Fig. 17. The calculated values of Gibbs free energy (ΔG), and the equilibrium constant (K_{eq}), for the chemical reactions (1), (2), (3) and (6) are shown in Table 3. From the data in Table 3, it is evident that K_{eq} is higher for the chemical reactions (1) and (2) at the exposure temperatures.

The lowest ΔG values of chemical reactions (1) and (2) indicate that the oxidation of SiC and Si-B-C (B_4C in the Si-B-C layer) has a greater thermodynamic driving force compared to that for the oxidation of carbon fibres and PyC interphase layer (difference being more at 1250 and 1400 °C), leading to the formation of the self-healing borosilicate glass, such that the carbon fibres are protected from degradation.

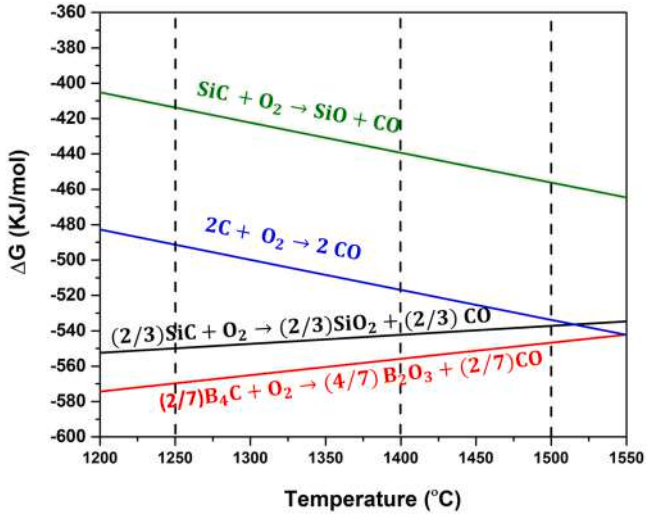

Fig. 17. Temperature dependence of the Gibbs free energy change per mole of oxygen (ΔG) for oxidation reactions occurring within the C_f/SiC composite exposed to high temperatures.

Furthermore, lower Gibbs free energy (ΔG) for the formation of SiO_2 compared to SiO (g) indicates a greater tendency for the formation of former oxide at the investigated test temperatures. Nevertheless, the free energy change for the chemical reaction (6) is also dependent on the oxygen partial pressure, which is expected to be ~0.21 at the oxide-air interface and decreases progressively with increasing depth beneath the surface. It has been previously reported that at a lower partial pressure, the SiC oxidises to form SiO (g) at a temperature > 1400 °C [31,42,45,46].

4.3. Oxidation behaviour

As the CO (g) is formed by oxidation of both carbon fibres and SiC/SiBC matrix according to the Reactions (1) - (3), its amount is intuitively expected to exceed that of B_2O_3-SiO_2 at a given instant, as the latter product is formed by oxidation of the matrix constituents only. As a result, the B_2O_3-SiO_2 scale needs to grow and self-heal at a faster rate compared to that of CO(g) formation, which in turn depends on the kinetics of oxygen ingress. Therefore, besides the thermodynamic feasibility, the kinetics of all the aforementioned reactions play a major role in the evolution of the B_2O_3-SiO_2 oxide scale, including its formation, stability, as well as protective and self-healing character. As a result, both mass-change as well as the oxide scale evolution mechanism strongly depend on both temperature and duration of exposure, and the nature of such correlation is a function of the carbon fibre architecture too, as discussed further in this section.

4.3.1. Non-isothermal oxidation

The results of the non-isothermal oxidation test are helpful for understanding the progress of oxidation during heating, which precedes the evolution of oxide scale during subsequent isothermal holding at a given temperature. As demonstrated by the thermogravimetric test results (Fig. 2), neither the 2.5D nor the 3D composite has exhibited a substantial mass loss up to 600 °C. However, beyond this temperature, both the composites have experienced a pronounced decrease in mass, suggesting a typically accelerated oxidation of the carbon fibres occurring above this critical temperature. As shown in Fig. 2, the rate of mass loss is higher in the 3D C_f/SiC composites compared to the 2.5D C_f/SiC composites, likely due to the increased porosity of the 3D NOOBed composites. Previous studies have reported that the oxidation of carbon fibres is initiated above ~550 °C, and its rate increases with temperature [47,48]. At 1100 °C, a slight mass gain is recorded for the 2.5D C_f/SiC composites due to the formation of SiO_2 (s) as described by Reaction 1. Previous studies have also shown that at temperatures exceeding 1100 °C, the oxidation kinetics of SiC is enhanced, leading to the formation and growth of a SiO_2 scale that serves as a protective barrier for the ingress of oxygen [45,49]. In contrast, the mass loss has been found to persist in the 3D C_f/SiC composites even after 1100 °C, suggesting continued oxidation of the carbon fibres. However, a slower rate of mass

Table 3
Thermodynamic data for the chemical reactions involved in the formation of oxide scale on 2.5D and 3D C_f/SiC composites.

No	Reactions	ΔG (KJ/mol)			K_{eq}		
		1250 °C	1400 °C	1500 °C	1250 °C	1400 °C	1500 °C
1	$(2/3)SiC(s) + O_2(g) \rightarrow (2/3)SiO_2(s,l) + (2/3)CO(g)$	−550	−542	−537	7.29×10^{18}	8.57×10^{16}	6.73×10^{15}
2	$(2/7)B_4C(s) + O_2(g) \rightarrow (4/7)B_2O_3(l) + (2/7)CO(g)$	−570	−556	−547	3.47×10^{19}	2.27×10^{17}	1.28×10^{16}
3	$2C(s) + O_2(g) \rightarrow 2CO(g)$	−491	−517	−534	7.12×10^{16}	1.38×10^{16}	5.35×10^{15}
4	$SiC(s) + O_2(g) \rightarrow SiO(g) + CO(g)$	−413.7	−439.3	−456.2	1.55×10^{14}	5.2×10^{13}	2.77×10^{13}

loss recorded for the 3D C_f/SiC composite at temperatures > 1100 °C could be attributed to the mass gain by the rapid formation of SiO_2 (s). However, the SiO_2-rich oxide scale does not act as an effective protective barrier to inhibit the oxidation of the 3D C_f/SiC composites due to their higher pore volume.

4.3.2. Cyclic oxidation

As shown in Fig. 3, the masses of the composites have decreased, indicating the occurrence of continuous mass loss with an increase in the duration of cyclic exposure for both 2.5D and 3D C_f/SiC composites. However, as shown in Fig. 3(d), the net mass loss recorded for these composites is dependent on both the carbon fibre architecture as well as the temperature of exposure. For the 2.5D C_f/SiC composites, the mass change exhibits a nearly linear variation with the exposure time. On the contrary, the mass change curves recorded for the 3D C_f/SiC composites resemble a negative parabola, indicating a sharper decrease with time of exposure beyond 60 h. As shown in Fig. 3(d), the mass loss observed in the 3D C_f/SiC on cyclic exposure at 1250 °C, 1400 °C and 1500 °C is respectively, 9.5, 90 and 7 times greater than that in the corresponding 2.5D C_f/SiC composite samples exposed at the same temperatures, indicating the factor of difference at 1400 °C to be higher by an order of magnitude. Furthermore, the standard deviation of mass loss recorded for the 3D C_f/SiC composite is greater compared to the 2.5D C_f/SiC composite, as shown in Fig. 3(d). When combined with the observed strength retention, the findings on mass change confirm that the 2.5D fibre architecture provides much superior oxidation resistance as well as higher strength retention compared to that present in the NOOBed 3D C_f/SiC composites.

4.3.3. Effect of fibre architecture on oxidation behaviour

More rapid mass loss along with a much larger standard deviation recorded for the NOOBed 3D C_f/SiC composite in comparison to the 2.5D C_f/SiC composite can be attributed to a much higher amount of porosity in the former composite, as discussed in an earlier report [29]. A detailed study using X-ray micro-CT has revealed the amount of inter-fibre porosity in the 3D C_f /SiC composite to be higher by 5 times compared to that of the 2.5D C_f /SiC composites (Table 1). Additionally, the 3D C_f/SiC composite contains inter-bundle pores with larger volumes (0.7–1.1 mm^3) than those observed in the 2.5D C_f/SiC composite. It is therefore intuitive to postulate that a higher amount of porosity present in the NOOBed 3D C_f/SiC composite have permitted an enhanced ingress of oxygen, finding its way through the defects in the SiO_2 scale and the SiC seal coating. It is intuitive that the penetration of oxygen beneath the outer SiO_2 scale and SiC seal coating (as confirmed by the results of ToF-SIMS depicted in Figs. (11–13) has caused accelerated oxidation of the carbon fibres accompanied by mass loss. Considering the preferential oxidation of C-fibres as well as of the carbon in the $(PyC/SiC)_{n=4}$ multilayered interphase (after oxidation of SiC-seal coating), it is intuitive that the resulting mass loss due to formation and escape of CO (g) would create discontinuities at the C_f/SiC interfaces. Therefore, in addition to inter-fibre and inter-bundle porosity (as discussed above), the distribution of C-fibres as well as the C_f/SiC interfacial area occupied by $(PyC/SiC)_{n=4}$ along the three principal directions, plays a crucial role in the extent of direction-specific damage by oxidation along with the consequent penetration of oxygen. As shown in Table 1, in the 2.5D C_f/SiC composite, the volume fractions of C-fibres in the x- and y-directions are 19.94 % each, whereas in the z-direction, it is only 0.12 %. In contrast, the 3D C_f/SiC composite exhibits C-fibre volume fractions of 10.9 % in both the x and y directions and 13.9 % in the z direction.

The net interfacial area per unit volume, assuming a circular cross-section of the fibres, can be deduced from the volume fraction of C-fibres that are aligned in each of the mutually orthogonal directions. For the calculation of interfacial area per unit volume, both 2.5D C_f/SiC and 3D C_f/SiC are considered as cubes with a volume of 1 mm^3 and dimensions 1 mm× 1 mm× 1 mm. Considering the carbon fibre as a cylindrical structure with a diameter (d) of 6.4 μm and length of 1 mm, the interfacial area and volume of a single carbon fibre have been found by calculating the values of πd and $0.25\pi d^2$, respectively. The method used to determine the interfacial area per unit volume of the C_f/SiC composite is described as follows.

Based on the aforementioned C-fibre volume fraction in x-direction of the 2.5D C_f/SiC composites, number of fibres aligned in x-direction (n_x) for 2.5D C_f/SiC composite has been found as ~6198 by dividing the volume of carbon fibres in x-direction (0.1994 mm^3) by the volume of a single carbon fibre in x-direction ($0.25\pi d^2 = 32.2 \times 10^{-6}$ mm^3). Therefore, the interfacial area per unit volume of carbon fibres aligned in the x-direction of the 2.5D C_f/SiC composite has been determined by multiplying the interfacial area of C-fibre per unit volume ($\pi d = 20.1 \times 10^{-3}$ mm^{-1}) by n_x (~6198), and found as 124.6 mm^{-1}. Similarly, using the previously mentioned carbon fibre volume fractions, interfacial area per unit volume for the 2.5D C_f/SiC composite in y- and z-directions has been found to be approximately 124.6 mm^{-1} and 0.75 mm^{-1}, respectively. Furthermore, the interfacial areas per unit volume of the 3D C_f/SiC composite have been calculated as 68 mm^{-1} in the x- and y-directions, and 86.9 mm^{-1} in the z-direction.

Notably, both the carbon fibre volume fraction as well as the interfacial area in the z-direction of the 3D C_f/SiC composite are ~115 times greater than that of the 2.5D composite. It is intuitive that the inward oxygen flux at the oxide-air interface of both 2.5D and 3D C_f/SiC composites would be identical on the surfaces perpendicular to the x, y and z directions. As the carbon fibres and the PyC in the interphase are preferentially oxidized, their minimal presence along the z-direction of the 2.5D C_f/SiC composite is considered to have lowered its susceptibility to oxidation. The oxygen penetrating along z-direction of the 2.5D C_f/SiC composite after the oxidation of SiC seal coating is expected to encounter layers of SiC/SiBC matrix as well as the PyC/SiC interphase prior to the carbon fibre bundles in a given x-y plane. On the contrary, the oxygen reaching beyond the oxidized SiC seal coating along the z-direction of 3D C_f/SiC composite would have direct encounter with carbon fibres and PyC/SiC interphase, which would lead to preferential oxidation of both the carbon fibres as well as the PyC at the interphase. As a result, the ingress of oxygen as well as oxidation along z-direction would be more rapid in the 3D C_f/SiC composite compared to the 2.5D C_f/SiC composite. Therefore, it is appropriate to consider that a substantially higher volume fraction of carbon fibre, as well as a larger interfacial area along the z direction of the 3D C_f/SiC composite along with its higher internal porosity content [29], have not only led to greater oxidation with mass loss, but also a deeper and more rapid penetration of oxygen compared to the 2.5D C_f/SiC composite. Additionally, it is inferred that the net oxidation rate of the investigated composites is determined by the synergistic effect of the directional

distribution of C-fibres, the net C_f/SiC interfacial area, as well as the interconnected inter-bundle and inter-bundle pores, all of which appear to collectively control the ease with which oxygen can penetrate the composite.

As already discussed in Section 4.1, the mass change in both 2.5D and 3D C_f/SiC composites depends on the oxidation products formed according to the chemical reactions (1) -(6). Higher mass loss observed in the case of the 2.5D C_f/SiC composites cyclically exposed at 1250 °C compared to that at other temperatures may be ascribed to the sluggish kinetics of SiO_2 formation at this temperature. In comparison to the observations on cyclic exposure of the 2.5D C_f/SiC composite samples at 1250 or 1500 °C, the lower mass change recorded at 1400 °C suggests that the formation of protective B_2O_3-SiO_2 scale has occurred fast enough to inhibit the ingress of oxygen. On the other hand, the observed increase of mass loss at 1500°C may be ascribed to the active oxidation of SiC to form SiO (g) along with the accelerated kinetics of C-fibre oxidation.

4.3.4. *Effect of temperature on oxidation behaviour*

Evaluation of oxidation kinetics from the mass loss curve using the conventional method of finding the rate constant may not be appropriate for C_f/SiC composites, because both mass gain and loss mechanisms are involved simultaneously to different degrees. Therefore, the rate of net change in mass with duration of cyclic exposure has been analysed to distinguish between different regimes of oxidation and oxide scale growth. The plots depicting the variation in the rate of mass change (resultant of mass gain and loss processes) in 2.5D and 3D C_f/SiC composites with the duration of cyclic exposure are shown in Fig. 18(a) and (b), respectively. The y-axis data for 2.5D and 3D C_f/SiC composites in Fig. 18 have been obtained by calculating the instantaneous slope in the plots of mass change against the time of cyclic exposure, as shown in Fig. 3(a-c). As shown in Fig. 18(a) and (b), the mass change behaviour of both 2.5D and 3D C_f/SiC composites varies with the temperature of cyclic exposure. Of course, such an observation regarding the mass loss is intuitive, considering that the evolution of oxide scale would depend on the temperature as well. As shown in Fig. 18, the oxidation of both 2.5D and 3D C_f/SiC composites appears to have progressed in two distinct stages exhibiting sharply different rates, with the first 40 h of exposure being categorised as Stage I and the rest as Stage II.

As shown in the plot obtained for the 2.5D C_f/SiC composite tested at 1250 °C (Fig. 18(a)), the rate of mass loss is the highest (highest negative value) initially and decreases sharply in the initial 20 h of exposure, after which it decreases gradually to reach the lowest value (~0.01 % h^{-1}) at a duration of 40 h. In the next stage (Stage II), the rate of mass loss remains more or less stable up to a duration of 70 h, after which it exhibits a gradual increase till 80 h of exposure, and an accelerated increase beyond this duration. The variation of mass loss rate observed for the 2.5D Cf/SiC composite with the duration of cyclic exposure at 1250 °C as shown in Fig. 18(a), is correlated with the oxide scale evolution through the following explanations: (i) the highest rate of mass loss recorded for the 2.5D C_f/SiC composite at the beginning of exposure at 1250 °C is ascribed to the preferred and rapid oxidation of carbon fibres, because of which the amount of CO (g) formed exceeds that of B_2O_3 (l) and SiO_2 (s); (ii) after ~20 h of exposure, formation and escape of CO (g) is restricted at least partially by the growth of B_2O_3-SiO_2 scale due to the continued oxidation of the surrounding SiC/SiBC matrix through the Reactions (1), (2) and (4), because of which the rate of mass loss is reduced leading to the emergence of a stable regime; (iii) the reduction of slope followed by a stable regime observed from 20 to 70 h of exposure suggests that the mass loss by the formation of CO (g) is balanced by the mass gain due to the growth of B_2O_3-SiO_2 scale, indicating that a dynamic equilibrium is reached; (iv) minor increase or decrease in the rates of mass loss within the stable regime of Stage II (until 70 h) indicates that the equilibrium between the processes of mass gain and loss is unstable, as the B_2O_3-SiO_2 scale is continuously ruptured and subsequently self-healed repeatedly; (v) the rupture of the oxide scale may not only permit the escape of residual CO (g) formed by the oxidation of carbon fibres, but also the ingress of oxygen from the air, leading to further oxidation and unstable regime observed beyond 80 h of exposure; and (vi) the accelerated rate of mass loss beyond 80 h of exposure indicates that the formation of CO (g) is much faster than the rate at which the B_2O_3-SiO_2 can grow and heal itself.

The mass loss recorded for the 2.5D C_f/SiC is almost close to zero on cyclic exposure at 1400 °C, unlike that observed at 1250 or 1500 °C, as illustrated in the plots shown in Fig. 3(a) through (c). During the cyclic exposure of 2.5D C_f/SiC composite at 1400 °C, the rate of mass change with time exhibits only a minor negative deviation from zero in Stage I, whereas it remains close to zero in Stage II (Fig. 18(a)). This observation for exposure at 1400 °C indicates that initially a small fraction of the carbon fibre is oxidised, and as time progresses, the rate of oxidation of SiC into SiO_2 and Si-B-C to SiO_2 and B_2O_3 increases, which leads to the formation of a protective scale in Stage II. The stability of mass change observed in Stage II confirms the ability of borosilicate glass formed by oxidation to flow and mask the pores and cracks in the oxide scale of the 2.5D C_f/SiC composite at 1400 °C, and thereby reduce the ingress of oxygen.

However, for the 2.5D C_f/SiC composite samples exposed at 1500 °C, a slight increase in the rate of mass loss is observed in Stage I, followed by a decrease in the rate of mass loss up to 80th h, which indicates that mechanisms of protective scale formation similar to that at 1400 °C are operative. However, after exposure for 80 h at 1500 °C, an increase in the rate of mass loss is observed in contrast to the behaviour observed at

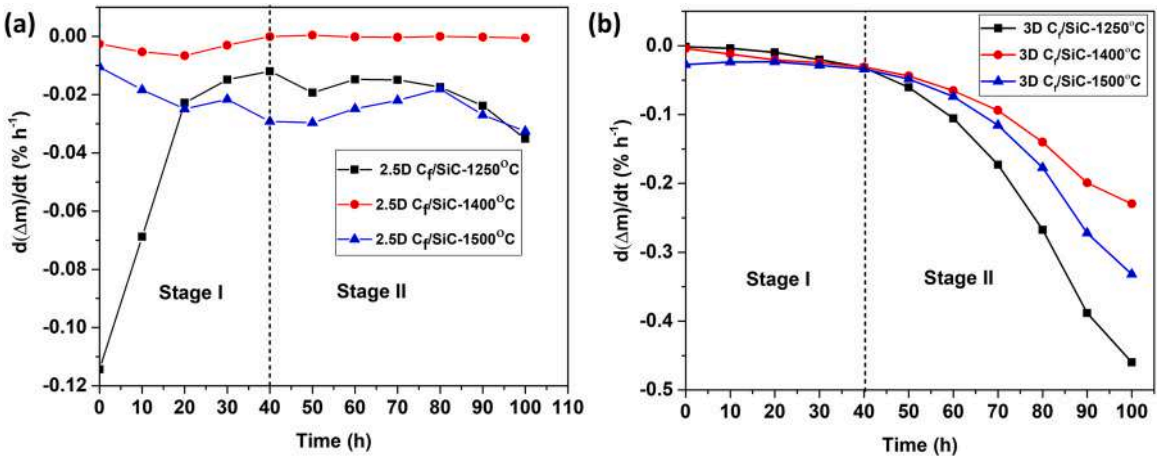

Fig. 18. Plots depicting how the rate of mass change varies with the duration of cyclic exposure for (a) 2.5D C_f/SiC and (b) 3D C_f/SiC composites.

1400 °C, which may be ascribed to active oxidation of SiC with the formation of SiO (g) according to the Reaction (6). The formation and escape of gaseous products, SiO (g) and CO (g), at 1500 °C may be considered responsible for the formation of pores in the SiO_2-rich oxide scale, as shown in the SEM image of the oxide scale cross section in Fig. 6 (c). Although the oxygen is able to penetrate and reach the oxide-SiC interface, yet its local partial pressure is expected to be less than ~0.21 atm by an order of magnitude or less, which explains why the active oxidation of SiC is promoted causing the formation of SiO (g), as reported in the literature [31,42,50]. Large cavities (Fig. 6(c) and (f)) found in the SiC matrix after cyclic oxidation for 100 h at 1500 °C are considered to further confirm the formation and escape of SiO (g) along with CO (g). In fact, coalescence of the finer neighbouring pores with growth in their size is also a possibility, considering that the surface area to volume ratio is progressively reduced as a consequence.

Unlike the 2.5D C_f/SiC composites, the rate of mass change calculated for the 3D C_f/SiC composite samples exhibits a similar pattern at all temperatures investigated, as shown in Fig. 18(b). The following inferences can be drawn from the plots depicted in Fig. 18(b): (i) during the first 40 h of exposure comprising Stage I, the rate of mass loss remains close to zero, which suggests that the native SiO_2 scale formed on the SiC seal coating is fairly protective and does not permit the oxygen to reach the carbon fibres; and (ii) after 40 h of exposure (Stage II), the rate of mass loss has increased significantly. Accelerated oxidation on subjecting to multiple cycles (~6) of 10 h exposure, indicates that both thermal and growth stresses may have led to the formation and interlinking of cracks in the SiO_2-rich oxide scale, which in turn is considered responsible for its partial rupture and spallation (Fig. 7(a)), allowing greater ingress of oxygen. Enhanced oxygen penetration within the matrix of 3D C_f/SiC composites is attributed partly to the presence of larger pores spanning a broad size range (0.7–1.1 mm^3) and increased inter-fibre porosity, as documented previously for 3D NOOBed composites [29]. In addition to the intrinsic porosity, two orders of magnitude higher volume fraction and interfacial area of the carbon fibres along the z-direction facilitates greater oxygen ingress. Also, the thermal shock caused by rapid cooling in air in between two consecutive heating cycles has probably led to high stresses caused by the difference between the thermal expansion coefficients of the oxide scale and their relaxation by the formation of cracks. The cracks formed in the oxide scale are expected to act as short-circuit paths for the ingress of oxygen, followed by accelerated oxidation of carbon fibres to form CO, resulting in an increase in the rate of mass loss. Moreover, during exposure at 1500 °C, the SiC is expected to undergo active oxidation, generating a mixture of SiO (g) and CO (g) gases (according to Reaction 6), as discussed in detail in the preceding paragraph. This reaction may have contributed to the additional mass loss observed at higher temperatures.

4.3.5. Evolution of oxide scale and its protective character

The XRD patterns obtained from the SiC seal coating and the cross-section of these composites (Fig. 4) after oxidation indicate that these composites have undergone limited sub-surface oxidation in addition to surface oxidation. The presence of SiO_2 has been detected both in the cross-section and at the surface of the seal-coated composites by using SEM-EDS and ToF-SIMS analyses. Based on the results obtained from the FESEM images depicting the oxide scales formed on the 2.5D C_f/SiC composites exposed at 1250 °C, the formation of cracks due to the stresses generated by the growth of oxides as well as the thermal stresses caused by repeated cycles of heating and cooling is evident on observing the oxide scale (Fig. 5(a)). The oxide scale formed is stable and does not show any sign of spallation, probably because the cracks are at least partially healed by the borosilicate glass formed by the oxidation of Si-B-C in the matrix. It is intuitive that the fluidity of borosilicate glass enables it to act as a cement and cause sinter-closure of the pores in the oxide scales of 2.5D C_f/SiC composites. From the cross-sectional image shown in Fig. 6(a), it is evident that the oxidation of carbon fibres has occurred to a very limited extent in the 2.5D C_f/SiC composites.

Contrary to the high structural integrity observed in oxide scales of the 2.5D C_f/SiC composite, the FESEM images depicting oxide scale surface and cross-section of the 3D C_f/SiC composites show evidence of a significant amount of spallation (Fig. 5(d) and Fig. 7(a)). Additionally, the extent of damage by oxidation of carbon fibre has been found to be much higher for the 3D C_f/SiC composite in comparison to the 2.5D C_f/SiC composite exposed at 1250 °C (Fig. 6(d)). Spallation of the oxide scale has occurred in case of the 3D C_f/SiC composites due to the defects (pores and cracks) generated by the escape of excess CO (g) formed by oxidation of carbon fibres as well as due to the thermal expansion mismatch between the oxide scale and the matrix underneath. Due to the presence of high porosity in the composite, the ingress of oxygen is higher for the 3D C_f/SiC composites, leading to the production of more gaseous products according to Reactions (1) to (3), whose escape has led to the spallation of their oxide scales [12,16].

As the temperature increases, the rate of SiO_2 formation increases, leading to the formation of a uniform oxide scale on 2.5D and 3D C_f/SiC composites at 1400 °C. The amount of oxidised carbon fibres is found to be negligible in the 2.5D C_f/SiC composite (Fig. 6(b)) and less compared to other temperatures in the 3D C_f/SiC composite (Fig. 6(e)). Based on the mass loss data depicted in Fig. 3 and the images of oxide scale cross-sections shown in Fig. 6 for cyclic exposure at 1400 °C for 100 h, it is inferred that oxide scale formed on the surface of 2.5D C_f/SiC composite is adequately protective against oxidation, whereas that on the 3D C_f/SiC composite is more stable in comparison to other temperatures. The formation of SiO_2 phase with globular morphology on the top surface is probably facilitated by the presence of B_2O_3 in the liquid state, whereas the existence of clusters suggests rapid growth of the B_2O_3-SiO_2 by non-uniform oxidation of the SiC and Si-B-C matrix as well as the SiC seal coating (Fig. 5(b) and (e)).

As discussed in Sections 4.1 to 4.3, the oxidation mechanism of both 2.5D and 3D C_f/SiC composite undergoes a noticeable change at 1500 °C, as the active oxidation of SiC becomes dominating and contributes to the formation of large cavities, as depicted in the SEM images of corresponding oxide scale cross-sections (Fig. 6(c) and (f)). Besides the active oxidation of SiC to form SiO (g), the oxidation of carbon fibre, interphase and matrix is also considered responsible for forming large cavities.

4.3.6. Role of boron in the evolution of oxide scale and its protective character

Oxide scale characterization with the help of depth profiling and spectroscopy (Figs. 10–13) using ToF-SIMS apparatus has revealed that for both 2.5D and 3D C_f/SiC composites, boron is present in the oxide scale formed on the surface of these composites, in spite of the Si-B-C layer being embedded within the SiC matrix underneath the SiC seal coating in the as-received composite, as shown in Fig. 1(c and d). The presence of boron both in the cross-section as well as at the surface of the oxide scale has been also confirmed by SEM-EDS analyses (Fig. 7). These observations indicate that the boron may have diffused through the grain boundaries within SiC matrix and seal coating to form B_2O_3 at the oxide/SiC interface. After its formation, the B_2O_3 (l) appears to have percolated towards the surface of the oxide scale by capillary action through an interlinked network of cracks and pores, which may have been subsequently sealed by the borosilicate glass, as illustrated in Figs. 6–7. Especially in the oxide scale formed on the NOOBed 3D C_f/SiC composite exposed at 1400 °C (Fig. 7(b)), the borosilicate glass appears to have sealed a majority of surface pores having a volume of ~0.7–1.1mm^3 [29].

Boron in the oxide scale plays a dual role. Firstly, the presence of B_2O_3 in borosilicate glass prevents its crystallisation to form cristobalite, and limits the path for interstitial diffusion of oxygen. Secondly, the bond length of B–O in borosilicate glass (~0.148 nm) is shorter than the Si-O bond in $[SiO_4^-]$ (~0.16 nm), which increases the activation energy for diffusion of molecular oxygen [51,52]. The defects such as bubbles and pits (Fig. 5(b) inset), formed in the borosilicate scale with increase

in its thickness due to the prolonged exposure at high temperatures, have been effectively healed by the borosilicate glass (Fig. 7(b) and (c)), as already discussed above. The increase in the B_2O_3 (l) content decreases the viscosity and therefore increases the flowability of the oxide scale, such that the cracks and pores are effectively sealed. At the same time, an increase in the temperature of exposure results in increased volatility of B_2O_3 (l) to form B_2O_3 (g), which in turn is expected to increase the amount of porosity in the oxide scale. Based on the trend observed for the mass loss data in Fig. 3, it is intuitive that sealing of discontinuities is most effective, making the oxide scale most protective at 1400 °C.

4.4. Post-cyclic oxidation flexural strength and fracture behaviour

The retention of strength by the investigated 2.5D and 3D C_f/SiC composites subjected to damage by thermal shock and partial oxidation by cyclic exposures at high temperatures with air-cooling is of interest for high-temperature load-bearing applications involving multiple cycles of heating and cooling. It has been noted that the stress-strain behaviour of these composites (Fig. 14(a) and (b)) is dependent on the temperature of exposure, porosity content, fibre architecture and the compliance of fibre-matrix interphase. The 2.5D C_f/SiC composite samples with lower porosity content, higher fibre volume fraction along the tensile axis as well as greater anisotropy compared to the 3D C_f/SiC composite (as discussed in detail in [29]) have exhibited higher flexural strength, as shown in Fig. 14(c). In spite of the temperatures of exposure being the same for both 2.5D and 3D C_f/SiC composites, the strength retained as a percentage of that in as-received condition is distinctly higher for the 2.5D C_f/SiC composite samples (~82–65 %) compared to the 3D C_f/SiC composite (~80–57 %). Also, it is interesting to note that compared to the 2.5D C_f/SiC composite, the standard deviations of flexural strengths determined at different test temperatures are greater for the 3D C_f/SiC composite samples, indicating the strong influence of high-volume porosities in the latter composite.

The retention of flexural strength by 2.5D and 3D C_f/SiC composites subjected to cyclic oxidation tests has been found to depend strongly on the protective character of the oxide scale formed. The 3D C_f/SiC composite cyclically exposed at 1250 °C for 100 h has been found to retain only 57 % of the strength exhibited in as-received condition primarily because of the non-protective character of its oxide scale, which has permitted an excessive ingress of oxygen as illustrated in Fig. 11(e) and (f), causing severe damage by oxidation. On the contrary, the presence of much smaller inter-bundle and inter-fibre pores in the 2.5D C_f/SiC composite due to the use of weaving and stitching techniques, has resulted in a more protective oxide scale at 1250 °C, enabling these composites to retain 82 % of their strength. However, significantly higher kinetics of SiO_2 formation at 1400 °C (in comparison to that at 1250 °C), has led to the formation of a more protective oxide scale (Figs. 8 and 9) compared to other temperatures, leading to significantly reduced damage by cyclic oxidation, along with much greater strength retention in both 2.5D and 3D C_f/SiC composites.

The stress-strain plots (Fig. 14) obtained from the three-point bend tests exhibit significant deviations from linearity as the typical characteristics of graceful or pseudo-ductile failure. Such a signature of graceful failure has been noticed even after multiple exposures of 100 h at 1250–1500 °C, indicating an impressive retention of the damage-tolerant capability. Furthermore, higher flexural strain observed in the case of the 3D C_f/SiC composite samples is suggestive of its greater damage tolerance compared to the 2D C_f/SiC composite. The examination of the fracture surfaces has shown evidence of interlaminar separation as the dominant mechanism of failure in the 2.5D C_f/SiC composite. On the contrary, the propagating crack is forced to interact with the continuous carbon fibres in 3D C_f/SiC along all three mutually orthogonal directions and undergo deflection, arrest or bridging, the effect of which is manifested as a more gradual decrease of the load-bearing capability after the peak in the flexural stress-strain curves.

A number of previous studies have focused on investigating the oxidation behaviour and evaluating the post-oxidation retained strength of the C_f/SiC composites subjected to varied processing and testing conditions. Lamouroux et al. have reported a strength retention of 66 % and 79 % after exposure at 700°C for 1.6 h and 1400°C for 0.5 h, respectively in a 2D C_f/SiC composite prepared through CVI [53]. For the 2.5D C_f/SiC composite samples with PyC interphase prepared via CVI, strength degradations of ~45–54 % and ~80 % have been reported after isothermal exposure for 1–4 h at 1300 °C and 1500 °C, respectively. The same composite has exhibited a mass loss of around 20 % after 4 h of isothermal exposure at 1500 °C [54]. Additionally, a study conducted on the 2D C_f/SiC composite with CVD-processed seal coatings of SiC and Si-B-C/SiC has exhibited strength retention of 79 % and 89 % respectively, after cyclic exposure at 1300 °C for 50 h [55]. However, a 2D C_f/SiC composite possessing a matrix of SiC/SiB_4 has exhibited degradation of flexural strength by ~28.5 % after isothermal exposure at 1000 °C for 10 h [15].

Previous studies have reported varied oxidation behaviour and strength retention in the 3D C_f/SiC composites depending on both the temperature and the duration of exposure. For instance, a 3D C_f/SiC composite prepared through CVI has exhibited a strength retention of ~45 % and a mass loss of ~10 % on isothermal exposure at 1250 °C for 3 h, with the mass loss being attributed to the presence of pores and microcracks within the composite [56]. Similarly, for a 3D woven C_f/SiC composite with SiC seal coating, the strength retained after isothermal exposure at 1300°C for 10 h has been found as ~68 % [57]. In another study, a 3D C_f/SiC braided composite, with a PyC interphase of thickness ~200 nm, has been found to retain only ~44 % of the original strength after exposure at 1300°C for 15 h [58]. However, the 3D C_f/SiC composites with advanced protective coatings have demonstrated much superior strength retention. A previous study on the SiC/B/SiC coated 3D C_f/SiC (braided) composites has reported ~77 % of the strength being retained after isothermal exposure for 2 h at 1300 °C [35]. Similarly, a 3D C_f/SiC composite with an amorphous boron carbide coating has been reported to exhibit ~82.6 % of its strength after 100 h of isothermal exposure at 1200 °C with a net mass gain of ~0.14 %, whereas a braided 3D C_f/SiC composite with a multilayered CVD SiC coating and a graphitic B–C interlayer has retained ~80 % of its strength after 15 h of exposure at 1300 °C [19,59]. In contrast, a study on the NOOBed 3D C_f/SiC composite with PyC interphase prepared through a hybrid process (CVI+PIP), has shown the tensile strength at 1000 °C to be only ~28 % of that at room temperature (~178 ± 25.7 MPa), indicating that a considerable amount of internal damage has occurred by oxidation due to the absence of protective coating [60].

A comprehensive comparison with the aforementioned results from the literature suggests that the strengths retained in the presently investigated 2.5D and 3D C_f/SiC composites after a cyclic exposure of 100 h at 1250 °C, 1400 °C and 1500 °C are consistently higher than the values reported in a majority of earlier publications. Such a comparison of the retained strengths suggests that the formation of a protective borosilicate scale formed by oxidation of SiC seal coating and Si-B-C matrix, as well as the multilayered interphase together, have considerable influence on both strength retention capability and damage tolerant flexural behaviour of 2.5D and 3D C_f/SiC composites subjected to prolonged cyclic exposure at elevated temperatures.

A detailed investigation of the fracture surfaces of 2.5D and 3D C_f/SiC composites as shown in Figs. 15 and 16, respectively, can be used to have an understanding of how the failure mechanism has been affected by oxidation in the present study. In the flexural test samples pre-exposed cyclically at 1400 °C for 100 h (Figs. 15(b) and 16(a)) (marked by arrows), the crack path appears tortuous, caused by fibre pull-out and debonding. As shown in Fig. 6(b) inset, both the carbon fibres and the PyC interphase have been subjected to partial oxidation during cyclic exposure at 1400 °C, leading to mass loss. Weakening of the $(PyC/SiC)_{n=4}$ interphase by partial oxidation is expected to reduce the interfacial shear stress, which in turn would promote crack

deflection and fibre debonding, followed by fibre pull-out, thereby increasing the pseudo-ductile behaviour of these composites. A qualitative examination of the fracture surfaces obtained in samples pre-exposed cyclically at 1250 and 1400 °C, has exhibited a greater amount of fibre pull-out at the higher temperature. These results are similar to those observed on high-temperature tensile tests, which have led to an increase in the average length of pulled-out fibres caused by the weakening of the multi-layered interphase at the fibre-matrix interface [27,38,61]. However, in the fracture surface of the composite samples subjected to cyclic exposure of 100 h at 1500 °C (Fig. 15(c)), even though there is a significant amount of fibre pull-out, various cavities in the matrix can be seen (red ellipse), which appear to have been caused by the localized depletion of the SiC matrix through active oxidation, as discussed earlier in Sections 4.1–4.3. The presence of porosities in the matrix results in a larger effective surface area for further oxidation, leading to significant deterioration of the composites. Active oxidation of the SiC matrix combined with the oxidation of carbon fibres and PyC layer are considered to have resulted in lower strength retention of 65 % by the 2.5D C_f/SiC composite exposed at 1500 °C.

Between 2.5D C_f/SiC and 3D C_f/SiC composite samples subjected to cyclic exposure at 1250 °C for 100 h, the latter composite has undergone catastrophic failure without being able to withstand the load. This observation suggests that the porosity introduced during NOOBing fabrication of the carbon fibre preform for the 3D C_f/SiC composites, has resulted in significant internal damage by the oxidation of carbon fibres, leading to brittle failure. The self-healing capability of the B_2O_3-SiO_2 contributed by the oxidation of SiBC matrix has been found to be inadequate for filling cracks and pores generated during the cyclic exposure of 3D C_f/SiC composite at 1250 °C. Furthermore, a substantial amount of oxide scale spallation has been observed in the oxide scale formed at this temperature (Fig. 5(d) and Fig. 7(a)). Such an extensive damage in the 3D C_f/SiC composite on cyclic exposure for 100 h at 1250 °C is considered responsible for its lower strength retention of 57 % compared to the 82 % of the original strength retained by the 2.5D C_f/SiC composites subjected to identical oxidation tests. Contrary to the large difference between the drop in flexural strengths of 2.5D and 3D C_f/SiC composites on cyclic exposure at 1250 °C, the reduction in flexural strengths of 2.5D and 3D C_f/SiC composite samples tested at 1400 °C and 1500 °C appear to be similar, as shown in Fig. 14(c). These observations suggest that the NOOBed 3D C_f/SiC composite is not suitable for use in load-bearing applications, if it is subjected to cyclic exposure at 1250 °C.

Plots depicting the variations of oxide scale thickness and retained strength with the temperature of cyclic exposure for 2.5D and 3D C_f/SiC composites are shown in Fig. 19(a) and (b), respectively. Based on the trend observed in Fig. 19(a) and (b), it is inferred that for an increase in the temperature of cyclic exposure from 1250 to 1400 °C, the oxide scale thicknesses of both 2.5D and 3D C_f/SiC composites have increased by ~25 % and ~92 %, respectively indicating sharp differences between their growth rates. An increase in the oxide scale thickness with the increase in the temperature of cyclic exposure from 1250 to 1400 °C is of course, well-expected considering the enhancement in the oxidation rate of SiC seal coating and matrix with temperature, which is also associated with a higher rate of SiO_2 formation and growth. As a result, for both 2.5D and 3D C_f/SiC composites, the SiO_2-rich scale evolved at 1400 °C has greater continuity and protective ability compared to that formed at 1250 °C. The greater rate of SiO_2 formation and its protective ability is also consistent with the lower mass loss recorded during exposure at 1400 °C compared to that at 1250 °C (Fig. 3(d)).

Although the oxide scale thicknesses observed on cyclic exposure at 1250 °C are comparable for 2.5D and 3D C_f/SiC composite, a significant difference has been found between their retained strengths (as a fraction of room temperature flexural strength), with the latter composite exhibiting much worse degradation. Greater degradation of the 3D C_f/SiC composite compared to the 2.5D C_f/SiC composite on cyclic exposure at 1250 °C is in tune with the fibre architecture of the former composite permitting greater ingress of oxygen. As already discussed in Section 4.3.3, the presence of larger volume of inter-fibre and inter-bundle pores, higher volume fraction of carbon fibres as well as larger fibre-matrix interfacial area along the z-direction, together result in greater ingress of oxygen in the 3D C_f/SiC composite compared to the 2.5D C_f/SiC composite. Penetration of oxygen to a greater depth in the 3D C_f/SiC composite cyclically exposed at 1250 °C, has not only resulted in greater internal damage by oxidation of carbon fibres, but also the formation of a thicker oxide scale compared to that observed in case of the 2.5D C_f/SiC composite (Table 2 and Fig. 19). The absence of (0002) carbon peak in the XRD pattern obtained from the oxide scale cross-section of the 3D C_f/SiC composite sample cyclically exposed at 1250 °C (as shown in Fig. 4(d) and its inset) may be considered as the credible evidence for substantial carbon fibre oxidation. On the contrary, the presence of (0002) carbon peak in the XRD pattern obtained from the oxide scale cross-section section of the 2.5D C_f/SiC composite sample cyclically exposed at 1250 °C (as shown in Fig. 4(c) and its inset) confirms that the carbon fibres underneath the SiO_2–rich top surface have been protected from oxidation. As a result of superior protection against damage by oxidation, the strength retained (as a percentage of flexural strength in as received condition) after cyclic exposure at 1250 °C is found to be far superior (44 % higher) for the 2.5D C_f/SiC composite compared to the 3D C_f/SiC composite (Fig. 19).

Considering that flexural strength and percentage retained strength (percentage of flexural strength found for as-received sample) of the 3D C_f/SiC composite sample exposed at 1400 °C are higher by 40 % each compared to the corresponding values obtained for the sample tested at 1250 °C (Fig. 19(b)), it is inferred that that oxide scale formed at the former temperature is more protective, and has restricted internal oxidation to a larger extent. It is intriguing to note the similarity

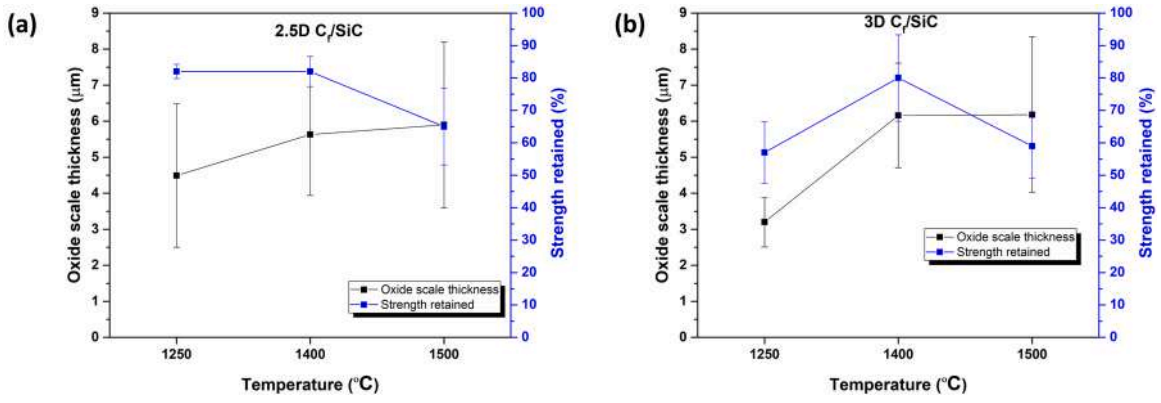

Fig. 19. Plots depicting the variation of oxide scale thickness and retained strength (percentage of flexural strength found for the corresponding as-received samples) with temperature for (a) 2.5D and (b) 3D C_f/SiC composite samples.

between the percentage retained flexural strengths of 2.5D and 3D C_f/SiC composites on cyclic exposure at 1400 °C in spite of much larger mass loss and higher increase in oxide scale thickness observed for the latter composite, as shown in Fig. 19(a) and (b). However, a comparison of the bar charts in Fig. 14(c) for the samples exposed cyclically at 1400 °C, indicates that the flexural strength of the 3D C_f/SiC composite is less than that of the 2.5D C_f/SiC composite by ~21 %, which is consistent with higher defect density and enhanced degradation accompanied by larger oxygen ingress and greater mass loss recorded for the former composite. Considering that the mass loss recorded for the 3D C_f/SiC composite is 90 times greater than that for the 2.5D C_f/SiC composite on cyclic exposure at 1400 °C (as shown in Fig. 3(d)), it is intuitive to expect the difference between the flexural strengths to be much greater than what has been shown in Fig. 14(c). It is therefore inferred that a fraction of the pores formed through mass loss during cyclic oxidation of the 3D C_f/SiC composite at 1400 °C may have been adequately healed by the borosilicate glass as shown in Fig. 7(b), such that the structural integrity is partially restored, and degradation of strength is minimized.

The results in Fig. 19(a) and (b) show that contrary to the behaviour noticed for increase in temperature from 1250 to 1400 °C, a further increase to 1500 °C has shown (i) a marginal increase in the oxide scale thickness of the 2.5D C_f/SiC composite, (ii) hardly any change in the oxide scale thickness of the 3D NOOBed C_f/SiC composite, and (iii) and a decrease in the percentage retained strength (percentage of flexural strength obtained in as-received condition) by 21 % for 2.5D and 26 % for 3D C_f/SiC composites with respect to the corresponding values observed in the samples exposed at 1400 °C. The sharp reduction in retained strength or negligible increase in the oxide scale thickness on increase of temperature from 1400 to 1500 °C may be ascribed to the combined effects of the following oxidation events: (i) active oxidation of SiC, (ii) oxidation of PyC/SiC interphase and carbon fibre, as well as (iii) the volatilization of B_2O_3, which have led to the formation of gaseous products, SiO (g), CO (g) and B_2O_3 (g). These gaseous products through their expansion and escape are considered to leave behind cracks and porosities in the oxide scale and the underneath composite, leading to the ingress of more oxygen along with accelerated oxidation.

Besides accelerated oxidation, the thermal shock caused by the multiple cycles of heating and cooling between 1500 °C and room temperature and the resulting thermal fatigue is also expected to contribute to the formation of cracks and their growth in both the oxide scale as well as the partially oxidized SiC matrix (beneath the oxide scale), leading to increased structural degradation of both 2.5D and 3D C_f/SiC composites. The strain caused by the thermal shock is proportional to (ΔCTE).(ΔT), where ΔCTE is the difference between the thermal expansion coefficients (CTE) of the composite and the SiO_2-rich oxide scale (CTE ~0.55×10^{-6} K^{-1}) [62,63], whereas ΔT is the difference between the maximum and minimum temperatures of each thermal cycle. Additionally, the thermal mismatch strain between the SiC matrix (CTE ~4.5×10^{-6} K^{-1}) [64] and the carbon fibres (longitudinal CTE ~1.6–2.1 $\times 10^{-6}$ K^{-1} and transverse CTE ~5–10 $\times 10^{-6}$ K^{-1}) [65] is expected to be significant due to not only the difference between their CTEs, but also the anisotropy between the CTEs along longitudinal and transverse directions. However, the presence of a compliant multi-layered interphase of $(PyC/SiC)_{n=4}$ and its partial oxidation is expected to minimise the CTE mismatch strain as well as the resulting damage. Considering that the thermal mismatch strain scales with the difference between maximum and minimum temperatures of each thermal cycle (ΔT), the thermal shock-induced damage on cooling is expected to increase with the maximum temperature of cyclic exposures, 1250 °C < 1400 °C < 1500 °C.

Due to the mismatch between the CTEs of C fibre and SiC matrix as described in the preceding paragraph, thermal residual stresses are generated in the composites during the cooling process from the processing temperature to room temperature during processing. Since the CTE of SiC matrix is higher than CTE of carbon fibre in the longitudinal direction, a compressive residual stress is generated in the fibre and a tensile stress is generated in the matrix [66,67]. The average thermal residual stress in the matrix of fibre reinforced CMC (0°/90°) is related to the processing temperature, T_p, by the following equation [54,68]:

$$\sigma_r = \frac{f_m E_T (E_L - E_m)}{(1+\nu)(E_T + E_L)} \quad (\alpha_f - \alpha_m)(T - T_p) \qquad \text{(ii)}$$

Here f_m is volume fraction of the matrix, E_m is the Young's modulus of the matrix, ν represents the Poisson's ratio of the composite, E_L and E_T are respectively, the longitudinal and transverse elastic modulus of the composites determined theoretically using the rule of mixtures and T is the temperature at which the composite is exposed. Based on Equation (ii), it is reasonable to expect that an increase in temperature would result in relaxation of the thermal residual stress generated by cooling the composite from the processing temperature. A survey of the previous literature suggests that relaxation in thermal residual stress leads to a significant improvement in the mechanical properties of the composites measured at high temperatures [38,54,69]. Henceforth, it is appropriate to infer that the effect of residual stress on the diffusion of oxygen and oxidising species within the composite, as well as the growth of self-healing B_2O_3-SiO_2 oxide scale is not significant.

Based on Equation (ii), it is also intuitive to predict that the thermal residual stress would be regenerated on cooling to the ambient temperature at the end of each heating cycle. Considering that compared to the 2.5D C_f/SiC composite, the volume fraction of carbon fibres as well as the interfacial area in the z-direction are much greater in the 3D C_f/SiC composite, it is appropriate to expect that the thermal residual stress and associated flaws (that is, microcracks and pores) in this direction would be much higher in the matrix of the latter composite. It is also reasonable to expect a significant increase in the matrix flaw size on subjecting the composites to multiple cycles of isothermal hold and cooling. Therefore, it is intuitive that after 10 cycles of high temperature exposure followed by cooling, the average size and density of flaws in the SiC matrix of the 3D C_f/SiC composite would be much greater than that in the 2D C_f/SiC composite. Due to the presence of higher density and size of flaws in the cyclic oxidation tested 3D C_f/SiC composite, its flexural strength is expected to be considerably less compared to the 2.5D C_f/SiC composite.

In the present study, the influence of oxidation rate and the evolution of oxide scale constituents appears to play a more dominant role than the thermal shock, which is evident from the least degradation of strength being observed after cyclic exposure at 1400 °C instead of the lowest temperature, 1250 °C. The lowest degradation of strength observed for both 2.5D and 3D C_f/SiC composite samples on cyclic exposure at 1400 °C is due to superior healing of matrix microcracks by the B_2O_3-SiO_2 glass compared to that at 1250 °C, which is responsible for an effective protection against damage by both oxidation and thermal shock. The ability of B_2O_3-SiO_2 glass to heal microcracks is expected to not only depend on its amount, but also on its viscosity and plasticity. It is rationale to consider that the viscosity of B_2O_3-SiO_2 glass would decrease, but its amount and plasticity would increase with increase in the oxidation test temperature, which can be used to explain superior microcrack healing at 1400 °C compared to that at 1250 °C. On the other hand, due to the combined influence of active oxidation of SiC as well as maximum CTE strain, the retained flexural strength of the 2.5D C_f/SiC composite has been found to be less after cyclic exposure at 1500 °C than that at 1400 or 1250 °C. However, for the 3D C_f/SiC composite, the retained flexural strengths observed after cyclic exposure at 1250 and 1500 °C appear to be nearly equal, indicating that the oxide scales formed at both these temperatures are almost equally non-protective.

5. Conclusions

The oxidation behaviour of CVI processed 2.5D (woven) and 3D (NOOBed) C_f/SiC composites have been studied by subjecting samples to 10 cycles of 10 h exposure (net duration of 100 h) at 1250 °C, 1400 °C and 1500 °C. The rate of mass change, the mechanism of oxidation as

well as the retained strength (percentage of flexural strength of as-received composite) after cyclic exposure at various temperatures have been examined. The key conclusions derived from the present study are:

1) Based on the variation of mass change with temperature during heating in the TGA, the temperatures for oxidation of carbon fibres (involving mass loss) and SiC matrix (involving mass gain) are found as $\geq$ 600 °C, and 1100 °C, respectively. The susceptibility for oxidation during non-isothermal exposure is much greater for the 3D C_f/SiC composite having shown 33 % greater mass loss than the 2.5D C_f/SiC composite.
2) The cyclic oxidation tests carried out for both 2.5D and 3D C_f/SiC composites have shown the net mass loss decreasing in the following order: 1250 °C> 1500 °C> 1400 °C. The net mass loss is more significant for the 3D C_f/SiC composite, being greater compared to the 2.5D composites by 9.5, 90, and 7 times at 1250°C, 1400°C, and 1500 °C, respectively. Thickness and defect density of the oxide scale are strongly influenced by both the temperature of exposure as well as the fibre architecture of these composites.
3) The variation of mass change with time in the 2.5D C_f/SiC composite follows a linear curve, whereas that recorded for the 3D C_f/SiC composite displays a negative parabola. Furthermore, the oxidation rate curves indicate two distinct stages. For the 2.5D C_f/SiC composite, oxidation mechanisms vary with the exposure temperature. In contrast, the rate of mass loss recorded for the 3D C_f/SiC composite is closer to zero in Stage I (up to 40 h), but increases sharply afterwards in Stage II.
4) The oxide scale thickness has increased with the temperature of exposure for both 2.5D and 3D C_f/SiC composites, indicating an enhancement in the kinetics of its growth. The oxide scale formed on 3D C_f/SiC composites has exhibited a substantial amount of spallation due to the formation and coalescence of porosity left behind by the escape of gaseous products (B_2O_3 and CO). The cracks and pores in the oxide scales act as the pathways of oxygen ingress till the oxide scale-composite interface.
5) The oxide scale is constituted by borosilicate glass, in which the presence of boron has been confirmed by ToF-SIMS mosaic mapping and depth profile. The oxide scale formed at 1400 °C is more stable and protective than that at other temperatures. The borosilicate layer, which has less viscosity than SiO_2 is effective in cementing the pores and microcracks, thereby arresting the inward penetration of oxygen.
6) On cyclic exposure at 1500 °C, the mass loss has increased due to the active oxidation of SiC being promoted by the reduction of oxygen partial pressure beneath the thick oxide scale. As the pores formed by active oxidation of SiC increase the effective area at the oxide-composite interface, the oxidation of carbon fibres is accelerated, leading to enhanced degradation of the composites.
7) Strength retained after 100 h of cyclic oxidation is the highest for exposure at 1400 °C, being 82 % and 80 % of the room temperature flexural strength for 2.5D and 3D C_f/SiC composites, respectively. Fractography has revealed increased fibre pull-out after high-temperature cyclic exposure, indicating weakening of the $(PyC/SiC)_{n=4}$ interphase due to the partial oxidation of PyC and carbon fibre. Superior flexural strength recorded for both 2.5D and 3D C_f/SiC composites after cyclic exposure at 1400 °C compared to that at 1250 °C confirms that the damage by oxidation and formation of a protective scale have a more significant influence than the thermal shock.
8) On cyclic exposure at 1250 °C, the retained strength of the 3D C_f/SiC composite (~57 %) is significantly less than that of the 2.5D C_f/SiC composite (~82 %), primarily due to greater damage by oxidation in the former composite with a larger amount of porosity content in as-received condition along with two orders of magnitude higher volume fraction and interfacial area of C-fibres in the z-direction. The adverse effect on the strength retention caused by cyclic exposure at 1500 °C for 100 h is similar for 2.5D and 3D C_f/SiC composites, as the active oxidation of SiC present in seal coating and matrix plays a dominant role in generating flaws.

CRediT authorship contribution statement

A. Udayakumar: Writing – review & editing, Supervision, Resources, Conceptualization. **Ramya Krishna:** Formal analysis, Data curation, Conceptualization, Writing – review & editing, Writing – original draft, Investigation. **Rahul Mitra:** Writing – review & editing, Supervision, Project administration, Funding acquisition, Conceptualization.

Declaration of Competing Interest

The authors declare that they have no known competing financial interests or personal relationships that could have appeared to influence the work reported in this paper.

Acknowledgements

The authors express their gratitude to Mr. L. Mariappan, Mrs. H.N. Roopa, Mr. P. Kumara and other technical staff of CSIR-NAL for material processing and to the Director, CSIR-NAL and Head, Material Science Division, CSIR-NAL, for providing C_f/SiC composite laminates. The authors acknowledge Mr. Mithun Das, Mr. B. Santu Mudliyar, Mr. Pradeep Guha and other staff members of Central Research Facility IIT Kharagpur and Department of Metallurgical and Materials Engineering IIT Kharagpur for their technical assistance in the characterisation of the specimens. Dr. Avinash Joshi and Mr. Uttam Garai of Sophisticated Analytical and Technical Help Institute (SATHI) Centre, IIT Kharagpur are gratefully acknowledged for their technical assistance in ToF-SIMS analysis on the specimens. The authors also thank the financial support from the Gas Turbine Materials and Processes (GTMAP) programme (Project No. 1848) of the Aeronautics Research and Development Board, Defence Research and Development Organisation (DRDO), New Delhi.

References

[1] R. Naslain, Design, preparation and properties of non-oxide CMCs for application in engines and nuclear reactors: an overview, Compos. Sci. Technol. 64 (2004) 155–170, https://doi.org/10.1016/S0266-3538(03)00230-6.
[2] R. Naslain, F. Christin, SiC-matrix composite materials for advanced jet engines, MRS Bull. 28 (2003) 654–658, https://doi.org/10.1557/mrs2003.193.
[3] W. Krenkel, F. Berndt, C/C-SiC composites for space applications and advanced friction systems, Mater. Sci. Eng. A. 412 (2005) 177–181, https://doi.org/10.1016/j.msea.2005.08.204.
[4] N. Al Nasiri, N. Patra, N. Ni, D.D. Jayaseelan, W.E. Lee, Oxidation behaviour of SiC/SiC ceramic matrix composites in air, J. Eur. Ceram. Soc. 36 (2016) 3293–3302, https://doi.org/10.1016/j.jeurceramsoc.2016.05.051.
[5] A. Udayakumar, M.R. Basha, S. Singh, S. Kumari, V.V.B. Prasad, Carbon Fiber Reinforced Silicon Carbide Ceramic Matrix Composites, in: Handb. Adv. Ceram. Compos, Springer International Publishing, Cham, 2020, pp. 877–911, https://doi.org/10.1007/978-3-030-16347-1_26.
[6] R.R. Naslain, The design of the fibre-matrix interfacial zone in ceramic matrix composites, Compos. Part A Appl. Sci. Manuf. 29 (1998) 1145–1155, https://doi.org/10.1016/S1359-835X(97)00128-0.
[7] J. Binner, M. Porter, B. Baker, J. Zou, V. Venkatachalam, V.R. Diaz, A. D'Angio, P. Ramanujam, T. Zhang, T.S.R.C. Murthy, Selection, processing, properties and applications of ultra-high temperature ceramic matrix composites, UHTCMCs – a review, Int. Mater. Rev. 65 (2020) 389–444, https://doi.org/10.1080/09506608.2019.1652006.
[8] F. Lamouroux, S. Bertrand, R. Pailler, R. Naslain, M. Cataldi, Oxidation-resistant carbon-fiber-reinforced ceramic-matrix composites, Compos. Sci. Technol. 59 (1999) 1073–1085, https://doi.org/10.1016/S0266-3538(98)00146-8.
[9] L. Vandenbulke, M. Leparoux, Silicon and boron containing components by CVD and CVI for high temperature ceramic composites, C5-735-C5-751, Le. J. Phys. 05 (1995), https://doi.org/10.1051/jphyscol:1995588.
[10] S.R.C.M. Tammana, V. Venkatachalam, J. Zou, M. Porter, J. Binner, Oxidation studies of SiC-coated 2.5D carbon fibre preforms, Open Ceram. 15 (2023) 100385, https://doi.org/10.1016/j.oceram.2023.100385.

[11] R. Naslain, A. Guette, F. Rebillat, R. Pailler, F. Langlais, X. Bourrat, Boron-bearing species in ceramic matrix composites for long-term aerospace applications, J. Solid State Chem. 177 (2004) 449–456, https://doi.org/10.1016/j.jssc.2003.03.005.

[12] M.R. Basha, A. Udayakumar, S.R. Sankaranarayanan, Synthesis and characterisation of Cf/SiC composites with modified silicon carbide matrix, Carbon Trends 5 (2021) 100082, https://doi.org/10.1016/j.cartre.2021.100082.

[13] Y. Liu, J. Wan, X. Zuo, L. Cheng, L. Zhang, Oxidation behavior of 2D C/SiC composites coated with multi-layer SiC/Si–B–C/SiC coatings under wet oxygen atmosphere, Appl. Surf. Sci. 353 (2015) 214–223, https://doi.org/10.1016/j.apsusc.2015.06.153.

[14] K.L. More, K.S. Ailey, R.A. Lowden, H.T. Lin, Evaluating the effect of oxygen content in BN interfacial coatings on the stability of SiC/BN/SiC composites, Compos. Part A Appl. Sci. Manuf. 30 (1999) 463–470, https://doi.org/10.1016/S1359-835X(98)00135-3.

[15] C. Tong, L. Cheng, X. Yin, L. Zhang, Y. Xu, Oxidation behavior of 2D C/SiC composite modified by SiB4 particles in inter-bundle pores, Compos. Sci. Technol. 68 (2008) 602–607, https://doi.org/10.1016/j.compscitech.2007.10.016.

[16] X. Luan, L. Wang, Y. Zou, Q. Zhang, R. Riedel, L. Cheng, Oxidation behavior of C/SiC-SiBCN composites at high temperature, J. Eur. Ceram. Soc. 39 (2019) 3003–3012, https://doi.org/10.1016/j.jeurceramsoc.2019.04.025.

[17] X. Luan, X. Xu, L. Wang, Y. Zou, R. Riedel, L. Cheng, Long-term oxidation behavior of C/SiC-SiBCN composites in wet oxygen environment, J. Eur. Ceram. Soc. 41 (2021) 1132–1141, https://doi.org/10.1016/j.jeurceramsoc.2020.09.058.

[18] J. Viricelle, P. Goursat, D. Bahloul-Hourlier, Oxidation behaviour of a multi-layered ceramic-matrix composite (SiC)f/C/(SiBC)m, Compos. Sci. Technol. 61 (2001) 607–614, https://doi.org/10.1016/S0266-3538(00)00243-8.

[19] Y. Liu, L. Zhang, L. Cheng, W. Yang, W. Zhang, Y. Xu, Preparation and oxidation protection of CVD SiC/a-BC/SiC coatings for 3D C/SiC composites, Corros. Sci. 51 (2009) 820–826, https://doi.org/10.1016/j.corsci.2009.01.026.

[20] U. A, S. M, V. K, Effect of CVD SiC seal coating on the mechanical properties of Cf/SiC composites generated through CVI, Surf. Coat. Technol. 219 (2013) 75–81, https://doi.org/10.1016/j.surfcoat.2013.01.007.

[21] S. Singh, V. Singh, S. Kumari, A. Udayakumar, V.V.Bhanu Prasad, Microstructural-property correlation of CVI processed Cf/SiC composites and property enhancement as a function of CVD SiC seal coating, Ceram. Int. 41 (2015) 14896–14907, https://doi.org/10.1016/j.ceramint.2015.08.020.

[22] M. RizvanBasha, A. Udayakumar, M. Stalin, S. Singh, V.V. Bhanu Prasad, S. R. Sankaranarayanan, Vapour phase synthesis and characterisation of Cf/SiC composites with self-healing Si-B-C monolayer coating, Ceram. Int. 46 (2020) 23785–23796, https://doi.org/10.1016/j.ceramint.2020.06.154.

[23] H. Yu, X. Zhou, W. Zhang, H. Peng, C. Zhang, Mechanical behavior of SiCf/SiC composites with alternating PyC/SiC multilayer interphases, Mater. Des. 44 (2013) 320–324, https://doi.org/10.1016/j.matdes.2012.07.073.

[24] R. Naslain, Recent advances in the field of ceramic fibers and ceramic matrix composites, J. Phys. 123 (2005) 3–17, https://doi.org/10.1051/jp4:2005123001.

[25] S. Singh, V. Singh, S. Kumari, A. Udayakumar, V.V.V.B. Prasad, A comparative study of tensile strength of Cf/SiC composites having single layer and multilayer interphases, Ceram. Int. 45 (2019) 21193–21199, https://doi.org/10.1016/j.ceramint.2019.07.099.

[26] R.R. Naslain, R.J.-F. Pailler, J.L. Lamon, Single- and multilayered interphases in SiC/SiC composites exposed to severe environmental conditions: an overview, Int. J. Appl. Ceram. Technol. 7 (2010) 263–275, https://doi.org/10.1111/j.1744-7402.2009.02424.x.

[27] R. Naslain, Fibre-matrix interphases and interfaces in ceramic matrix composites processed by CVI, Compos. Interfaces 1 (1993) 253–286, https://doi.org/10.1163/156855493X00112.

[28] Y. Jia, K. Li, L. Xue, J. Ren, S. Zhang, X. Zhang, Microstructure and mechanical properties of carbon fiber reinforced multilayered (PyC–SiC)n matrix composites, Mater. Des. 86 (2015) 55–60, https://doi.org/10.1016/j.matdes.2015.07.018.

[29] R. Krishna, P. Wilson, M.A. Williams, P. Srirangam, A. Udayakumar, R. Mitra, Effect of CVI-induced porosity on elastic properties and mechanical behaviour of 2.5D and 3D Cf/SiC composites with multilayered interphase, J. Eur. Ceram. Soc. 44 (2024) 4930–4948, https://doi.org/10.1016/j.jeurceramsoc.2024.02.039.

[30] L. Cheng, Y. Xu, L. Zhang, X. Luan, Oxidation and defect control of CVD SiC coating on three-dimensional C/SiC composites, Carbon 40 (2002) 2229–2234, https://doi.org/10.1016/S0008-6223(02)00103-3.

[31] E.J. Opila, J.L. Serra, Oxidation of carbon fiber-reinforced silicon carbide matrix composites at reduced oxygen partial pressures, J. Am. Ceram. Soc. 94 (2011) 2185–2192, https://doi.org/10.1111/j.1551-2916.2010.04376.x.

[32] Y. Deng, Y. Hao, C. Zhang, R. Wang, Fracture toughness evolution and failure mechanisms of two-dimensional SiCf/SiC composites at temperatures up to 1500 °C in air, Theor. Appl. Fract. Mech. 131 (2024) 104458, https://doi.org/10.1016/j.tafmec.2024.104458.

[33] X. Luan, L. Wang, Y. Zou, Q. Zhang, R. Riedel, L. Cheng, Oxidation behavior of C/SiC-SiBCN composites at high temperature, J. Eur. Ceram. Soc. 39 (2019) 3003–3012, https://doi.org/10.1016/j.jeurceramsoc.2019.04.025.

[34] R. Naslain, A. Guette, F. Rebillat, S. Le Gallet, F. Lamouroux, L. Filipuzzi, C. Louchet, Oxidation mechanisms and kinetics of SiC-matrix composites and their constituents, J. Mater. Sci. 39 (2004) 7303–7316, https://doi.org/10.1023/B:JMSC.0000048745.18938.d5.

[35] Y. Liu, L. Cheng, L. Zhang, S. Wu, D. Li, Y. Xu, Oxidation protection of multilayer CVD SiC/B/SiC coatings for 3D C/SiC composite, Mater. Sci. Eng. A 466 (2007) 172–177, https://doi.org/10.1016/j.msea.2007.02.059.

[36] F. Lamouroux, G. Camus, J. Thébault, Kinetics and mechanisms of oxidation of 2D Woven C/SiC composites: i, experimental approach, J. Am. Ceram. Soc. 77 (1994) 2049–2057, https://doi.org/10.1111/j.1151-2916.1994.tb07096.x.

[37] X. Cao, X. Yin, X. Ma, X. Fan, L. Cheng, L. Zhang, Oxidation behavior of SiBC matrix modified C/SiC composites with different PyC interphase thicknesses, Ceram. Int. 41 (2015) 1695–1700, https://doi.org/10.1016/j.ceramint.2014.09.111.

[38] R. Krishna, V.K. Parimi, A. Udayakumar, R. Mitra, Evaluation of elastic constants and high temperature tensile behaviour with damage assessment of the SiC seal-coated 2.5D Cf/SiC composites having multilayered interphase and Si-B-C added matrix, J. Eur. Ceram. Soc. 43 (2023) 2388–2401, https://doi.org/10.1016/j.jeurceramsoc.2022.12.066.

[39] N. Khokar, Noobing: A nonwoven 3D fabric-forming process explained, J. Text. Inst. 93 (2002) 52–74, https://doi.org/10.1080/00405000208630552.

[40] ASTM C1341-13, Standard Test Method for Flexural Properties of Continuous Fiber-Reinforced Advanced Ceramic Composites, ASTM Int. (2013). https://doi.org/10.1520/C1341-13.

[41] M. Hubert, A.J. Faber, On the structural role of boron in borosilicate glasses, Phys. Chem. Glas. Eur. J. Glas. Sci. Technol. Part B 55 (2014) 136–158. ⟨https://www.ingentaconnect.com/content/sgt/ejgst/2014/00000055/00000003/art00003⟩.

[42] S.K. Kashyap, K. Sala, R. Mitra, Oxidation resistance and evolution of multi-layered oxide scale during isothermal and cyclic exposure of ZrB2–SiC–LaB6 composites at 1300 °C to 1500 °C, Metall. Mater. Trans. A 53 (2022) 147–171, https://doi.org/10.1007/s11661-021-06501-4.

[43] J. Dai, L. He, R. Mu, Z. Xu, Z. Shen, R. Zhang, G. Liu, Oxidation behavior and damage mechanism of SiC f /SiC minicomposites with multilayered (BN/SiC) n interfacial coatings at 1200 ℃, Compos. Interfaces 30 (2023) 1–19, https://doi.org/10.1080/09276440.2022.2109795.

[44] I. Barin, Thermochemical Data of Pure Substances, Wiley, 1995, https://doi.org/10.1002/9783527619825.

[45] J. Roy, S. Chandra, S. Das, S. Maitra, Oxidation behaviour of silicon carbide - A review, Rev. Adv. Mater. Sci. 38 (2014) 29–39.

[46] N.S. Jacobson, D.L. Myers, Active oxidation of SiC, Oxid. Met. 75 (2011) 1–25, https://doi.org/10.1007/s11085-010-9216-4.

[47] Y. Yin, J.G.P. Binner, T.E. Cross, S.J. Marshall, The oxidation behaviour of carbon fibres, J. Mater. Sci. 29 (1994) 2250–2254, https://doi.org/10.1007/BF01154706.

[48] M.C. Halbig, J.D. McGuffin-Cawley, A.J. Eckel, D.N. Brewer, Oxidation kinetics and stress effects for the oxidation of continuous carbon fibers within a microcracked C/SiC ceramic matrix composite, J. Am. Ceram. Soc. 91 (2008) 519–526, https://doi.org/10.1111/j.1551-2916.2007.02170.x.

[49] L. Filipuzzi, R. Naslain, Oxidation Mechanisms and Kinetics of 1D-SiC/C/SiC Composite Materials: II, Modeling, J. Am. Ceram. Soc. 77 (1994) 467–480, https://doi.org/10.1111/j.1151-2916.1994.tb07016.x.

[50] P.E. Pehrsson, B.D. Thoms, Surface oxidation chemistry of β-SiC, J. Vac. Sci. Technol. A Vac. Surf. Film. 15 (1997) 1–9, https://doi.org/10.1116/1.580466.

[51] N.S. Jacobson, E.J. Opila, Oxidation and Corrosion of Non-oxide Ceramics, in: Encycl. Mater. Tech. Ceram. Glas, Elsevier, 2016, pp. 440–444, https://doi.org/10.1016/B978-0-12-818542-1.02350-X.

[52] M. Zhang, D. Li, Y. Hong, Z. Niu, Z. Yang, D. Jia, Y. Zhou, Study on the oxygen diffusion in the oxide layers of SiBCN ceramics by SIMS, J. Eur. Ceram. Soc. 42 (2022) 1341–1347, https://doi.org/10.1016/j.jeurceramsoc.2021.12.020.

[53] F. Lamouroux, G. Camus, Oxidation effects on the mechanical properties of 2D woven C/SiC composites, J. Eur. Ceram. Soc. 14 (1994) 177–188, https://doi.org/10.1016/0955-2219(94)90105-8.

[54] M. Patel, M.P.S. Kiran, S. Kumari, V. Singh, S. Singh, V.V.B. Prasad, Effect of oxidation and residual stress on mechanical properties of SiC seal coated C/SiC composite, Ceram. Int. 44 (2018) 1633–1640, https://doi.org/10.1016/j.ceramint.2017.10.085.

[55] X. Zuo, L. Zhang, Y. Liu, L. Cheng, Y. Xia, Oxidation behaviour of two-dimensional C/SiC modified with self-healing Si–B–C coating in static air, Corros. Sci. 65 (2012) 87–93, https://doi.org/10.1016/j.corsci.2012.08.003.

[56] X. Yin, L. Cheng, L. Zhang, Y. Xu, J. Li, Oxidation behavior of 3D C/SiC composites in two oxidizing environments, Compos. Sci. Technol. 61 (2001) 977–980, https://doi.org/10.1016/S0266-3538(00)00190-1.

[57] X. Yin, L. Cheng, L. Zhang, Y. Xu, X. Luan, Oxidation behaviour of three-dimensional woven C/SiC composites, Mater. Sci. Technol. 17 (2001) 727–730, https://doi.org/10.1179/026708301101510456.

[58] J.T. Hou, S.R. Qiao, C.Y. Zhang, Y.B. Zhang, The influence of high temperature exposure to air on the damage to 3D-C/SiC composites, Xinxing Tan. Cailiao N. Carbon Mater. 24 (2009) 173–177, https://doi.org/10.1016/s1872-5805(08)60046-3.

[59] S. Wu, L. Cheng, W. Yang, Y. Liu, L. Zhang, Y. Xu, Oxidation protective multilayer CVD SiC coatings modified by a graphitic B-C interlayer for 3D C/SiC composite, Appl. Compos. Mater. 13 (2006) 397–406, https://doi.org/10.1007/s10443-006-9025-8.

[60] A. Udayakumar, M.R. Basha, M. Stalin, V.V.B. Prasad, Mechanical properties of 3D noninterlaced Cf/SiC composites prepared through hybrid process (CVI + PIP), Int. J. Mater, Metall. Eng. 8 (2016) 1021–1028. ⟨https://zenodo.org/records/1096401⟩.

[61] J.K. Wells, P.W.R. Beaumont, Debonding and pull-out processes in fibrous composites, J. Mater. Sci. 20 (1985) 1275–1284, https://doi.org/10.1007/BF01026323.

[62] B. Deng, Y. Shi, F. Yuan, Investigation on the structural origin of low thermal expansion coefficient of fused silica, Materialia 12 (2020) 100752, https://doi.org/10.1016/j.mtla.2020.100752.

[63] W.E. Forsythe, et al., Smithsonian physical tables, Smithson. Misc. Collect (1954).

[64] Z. Li, R.C. Bradt, Thermal expansion of the cubic (3C) polytype of SiC, J. Mater. Sci. 21 (1986) 4366–4368, https://doi.org/10.1007/BF01106557.

[65] C. Pradere, C. Sauder, Transverse and longitudinal coefficient of thermal expansion of carbon fibers at high temperatures (300–2500K), Carbon 46 (2008) 1874–1884, https://doi.org/10.1016/j.carbon.2008.07.035.
[66] K.K. Chawla, Ceramic matrix composites, Springer Science & Business Media, 2013, https://doi.org/10.1007/978-1-4615-1029-1.
[67] H. Mei, H. Li, Q. Bai, Q. Zhang, L. Cheng, Increasing the strength and toughness of a carbon fiber/silicon carbide composite by heat treatment, Carbon 54 (2013) 42–47, https://doi.org/10.1016/j.carbon.2012.11.001.
[68] A.G. Evans, F.W. Zok, T.J. Mackin, The structural performance of ceramic matrix composites, High. Temp. Mech. Behav. Ceram. Compos (1995) 3–84, https://doi.org/10.1016/b978-075069399-8/50002-5.
[69] Y. Shi, F. Kessel, M. Friess, N. Jain, K. Tushtev, Characterization and modeling of tensile properties of continuous fiber reinforced C/C-SiC composite at high temperatures, J. Eur. Ceram. Soc. 41 (2021) 3061–3071, https://doi.org/10.1016/j.jeurceramsoc.2020.09.043.